NATIONAL RESEARCH COUNCIL OF ITALY
INSTITUTE OF MARINE SCIENCES
MARINE GEOLOGY SECTION (BOLOGNA)

JOINT RESEARCH PROJECT "GEOLOGY AND GEOPHYSICS OF THE ANDREW BAIN FRACTURE ZONE, SW INDIAN RIDGE"

NATIONAL ITALIAN ANTARCTIC PROJECT - CNR
GIN - RUSSIAN ACADEMY OF SCIENCES

REPORT ON THE MORPHOBATHYMETRIC, MAGNETOMETRIC, GRAVIMETRIC, REFLECTION SEISMIC AND DREDGING INVESTIGATIONS DURING CRUISE S23-AB06 ABOARD R/V STRAKHOV

ISMAR-CNR, Bologna (PNRA)
GIN-RAS, Moscow
SIO-UCSD, La Jolla and UNCW, Wilmington (NSF)
LDEO, New York
and
the S23-AB06 Survey Team

ISMAR Bologna - TECHNICAL REPORT N.100

Bologna, May 2006

ISMAR-CNR Cataloging-In-Publication data: ISMAR Bologna - TECHNICAL REPORT N.100

Report on the morphobathymetric, magnetometric, gravimetric, multichannel reflection seismic and dredging investigations during cruise S23-AB06 aboard R/V A.N.Strakhov.

by Ligi M., Bonatti E., Skolotnev S, Peyve A., Grindlay N.R., Sclater J., Bortoluzzi G., Brunelli D., Cipriani A., Mercuri R., Muccini F., Paganelli E., Zaffagnini F., Takeuki C., Baramykov Y., Chamov N., Erofeev S., Eskin A., Kolodyazhnyy S., Pertsev A., Semenov V., Rastorgyev V., Tsukanov N., Turko N., Yefimov V. and Zotov L.

Includes bibliographical reference and index.
1.SW Indian Ocean 2.Fracture Zone 3. Tectonics 5. Petrology 6. Geochemistry

Abstract - A summary of methodologies, technical details and ship-board results of a swath bathymetry, geophysical and geological survey in the Andrew Bain F.Z., SW Indian Ocean is presented. The cruise was done in a cooperative framework between PNRA and GIN-RAS, and utilized the *R/V Strakhov* of GIN-RAS. The F.Z. from 52S to 44S was investigated. During the survey, detailed, full coverage bathymetry, multichannel, single channel and SBP reflection seismic, magnetometric, gravimetric lines, bottom sampling were carried out in the Area.

Sommario - Vengono presentati le metodologie e l'insieme dei risultati ottenuti durante una campagna di rilievi batimetrici e geofisici nella zona di frattura Andrew Bain nell'Oceano Indiano occidentale. La crociera e' parte del Progetto nazionale Ricerche in Antartide, ed e' stata utilizzata la nave da ricerca *R/V Strakhov* del GIN-RAS. La zona della Frattura da 52S a 44S e' stata investigata. Si e' ottenuta una mappa batimetrica dettagliata con sistema 'multibeam', sono state fatte indagini di sismica a riflessione multicanale e SBP ad alta risoluzione, sono stati raccolti dati magnetometrici ed e' stato campionato il fondo marino .

Reproduced by ISMAR-CNR from camera-ready proofs supplied by the authors.
Published in the WWW at doc.bo.ismar.cnr.it and www.bo.ismar.cnr.it
Available in the HTML and PDF formats.Available also in other formats, upon request.
Hereafter a link to verbatim copy of this document (LATEX).

Production Notes - The document was edited with standard text editors, typeset with L.Lamport's LaTeX, translated to `PostScript` with `dvips` and printed with an A4 laser printer. The full production was done on a GNU Linux box with `GNU-GPL` software. Converted to HTML by N.Drakos's LaTeX2HTML and to `PDF` by Alladin Ghostscripts's `ps2pdf`. Most of the maps included were produced by Wessel and Smith's `GMT` package. Some drawings were produced by `xfig` (www.xfig.org). Non `PostScript` images were converted by John Bradley's `xv` or other public-domain packages, among them `convert`.

ACRONYMS

ACRONYM	DESCRIPTION	URL-email
PNRA	Progetto Nazionale Ricerche in Antartide	www.pnra.it
CNR	Consiglio Nazionale Delle Ricerche	www.cnr.it
RAS	Russian Academy of Sciences	www.ras.ru
ISMAR	Istituto di Scienze Marine	www.bo.ismar.cnr.it
GIN-RAS	Geological Inst., Moscow	www.ginras.ru
SIO-UCSD	Scripps Institute of Oceanography, UCSD	www.sio.ucsd.edu
UNCW	Univ. of North Carolina Wilmington	www.uncw.edu
LDEO	Lamont-Doherty Earth Obs., Columbia Univ.	www.ldeo.columbia.edu
UCSD	Univ.California S.Diego	www.ucsd.edu
NSF	National Science Foundation	www.nsf.gov
CEA-CNRS	Commissariat Energie Atomique, CNRS	www.cea.fr
CNRS	Centre National Reserche Scientifique	www.cnrs.fr
NSTU	Nizhny Novgorod state technical university	www.nntu.sci-nnov.ru
SIO	Shirshov Institute of Oceanology	www.sio.rssi.ru/index_en.htm
UNIMODENA	Univ. Modena	www.unim.it
UNIROMA	Univ Roma "La Sapienza"	www.uniroma.it
INGV	Ist.Naz.Geofisisica e Vulcanologia	www.ingv.it
IGEM-RAS	Institute Geology Ore Deposits, Petrography, Mineralogy and Geochemystry	www.igem.ru/igem/
ORMSP	Ocean Ridge Multibeam Synthesis Project	ocean-ridge.ldeo.columbia.edu
IAGA	Int.Ass.of Geomagnetism and Aeronomy	www.iugg.org/IAGA/
IGRF	Int.Geomagnetic Reference Field	www.ngdc.noaa.gov/IAGA/vmod/
INTERMAGNET	INTErn.Real-time MAGnetic Obs.NETwork	www.intermagnet.org
GEBCO	General Bathym.Chart Oceans	www.ngdc.noaa.gov/mgg/gebco
SGM	Satellite Gravity Maps	topex.ucsd.edu
SEG	Soc. of Exploration Geophysicists	www.seg.org
POR	(Eulerian) Pole of Rotation	encyclopedia.jrank.org/POL_PRE
SWIR	South Western Indian Ridge	
FZ	Fracture Zone	
ABFZ	Andrew Bain FZ	
DTFZ	Du Toit Fracture Zone	
MFZ	Marion Fracture Zone	
PEFZ	Prince Edward Fracture Zone	
RTI	Ridge Transform Intersection	
MAR	Mid Atlantic Ridge	
MBES	MULTIBEAM ECHOSOUNDER SYSTEM	
MCS	Multichannel Seismic	
SBP	Sub Bottom Profiling	
SVP	Sound Velocity Profile	
CTD	Conductivity/Temperature/Depth	
GPS-DGPS-RTK	Global Positioning System	samadhi.jpl.nasa.gov
DTM	Digital Terrain Model	en.wikipedia.org
RESON	Reson	www.reson.com
EDGETECH	Edgetech	www.edgetech.com
MARINE MAGNETICS	Marine Magnetics	www.mm.com
COMM-TEC	Communication Technology	www.comm-tec.com
NEPTUNE	Simrad MBES Software	www.kongsberg-simrad.com
MB-SYSTEM	MB-SYSTEM	www.ldeo.columbia.edu/res/pi/MB-System/
GMT	Generic Mapping Tool	gmt.soest.hawaii.edu/gmt
GNU,GPL	GNU is not Unix,General Pub. License	www.gnu.org

Table 1: Acronyms of Organizations, Manufacturers and Products

AUTHORSHIP

Giovanni Bortoluzzi compiled and finalized the main body of this report. M.Ligi, E.Bonatti, S.Skolotnev, A.Peyve, J.Sclater, N.Grindlay, A. Cipriani and D.Brunelli contributed to the geological and scientific background and to the preliminary data analysis. All the named participants to the cruise contributed to this report with their work and discussions aboard the *R/V Strakhov* .

HOW TO READ THIS REPORT

Sections 1 and 2 give the introductory and background information, including some technological and scientific issues of the organization and execution of tasks, whereas section 3 summarizes the cruise operations. Section 4 provides the technical aspects that were involved in the data acquisition and processing. Sections 5 and 6 discuss the initial results, the on-going data processing and usage, and give concluding remarks. Some data processing procedures that were used in the production of this report along with additional technical details and data are presented in the Appendix.

ACKNOWLEDGMENTS

Many people contributed to the success of the research cruise (S23-AB06 *R/V Strakhov*). Firstly, we wish to thank Captain Georgiy Chechyotkin, the Chief Engineer, the officers and crew members of *R/V Strakhov* for their professionalism and efforts in assuring the success of the cruise. The project was co-funded by Italy's PNRA project and Russia's GIN-RAS. Prof. C.A.Ricci, CNSA Commitee of PNRA and Dr. Vignato of ENEA/PNRA are warmly aknowledged for funding, assistance and handling of the Contract. The ISMAR team is indebted to the colleagues of Bologna, Dr.M.Ravaioli and P.Dall'Olio, for the continuous effort in resolving the financial and technical problems,

Contents

List of Figures

List of Tables

1 INTRODUCTION

The theory of plate tectonics has shown the Earth to be a dynamic system of shifting lithospheric plates, and the concept of transform faults, introduced by [Wilson (1965)], was one of the key steps in its development. Transform faults offset the axis of mid-ocean ridges and are the locus of strike slip motion at the boundary of the two plates that move sliding past each other. Although large-offset transforms such as the Romanche in the Equatorial Atlantic (longest in the world's oceans) formed the basis of this concept, recent geophysical data have revealed that this and another similar transform in the Southwest Indian Ocean, the Andrew Bain (second longest), do not lie on small circles about the Eulerian POR. An Italian research group of ISMAR-CNR of Bologna [Bonatti et al.(1994), Bonatti et a.(1996), Bonatti et al.(2001), Ligi et al.(2002)] propose that both the Romanche and Andrew Bain transforms represented a new class of oceanic transform boundaries, mega-transforms, "with broad, complex multifault zones of deformation similar to some continental strike-slip systems".

In the austral summer of 1996, Grindlay, Sclater and others carried out a marine geophysical survey (R/V Knorr, cruise KN145-L16) of the ultra-slow spreading Southwest Indian Ridge (Figs.1 and 2) that included a reconnaissance survey of the slowly slipping ABFZ [Grindlay et al.(1996), Grindlay et al.(1998), Sclater et al.(2005)].

The Italian research team proposed, jointly with GIN-RAS, to lead a marine geological and geophysical expedition to the same transform in austral summer 2005-2006, within the framework of the PNRA, and invited the Sclater and Grindlay teams to participate in the cruise, to share respective data and to collaborate in the post-cruise data analysis. The geological and geophysical data from the new expedition, when combined with data collected by Grindlay and Sclater, will provide a complete view of the morphology, tectonic fabric and physical structure of the Andrew Bain transform domain.

The PNRA approved fundings and a cruise was scheduled early 2005 with the GIN-RAS *R/V Strakhov* , with work at sea including multibeam, magnetic, gravimetric, seismic reflection surveys and rock sampling. In addition to processing and interpretation of the geophysical data obtained at sea, a comprehensive analytical program on the geochemistry of mantle and igneous rocks was also planned. The scientific objectives of the analysis of the geological and geophysical pointed:

- To define the morphology and structural framework and compare both with other slowly slipping mega-transforms and large continental strike-slip zones.
- To determine the composition of the Andrew Bain transform domain and investigate how the mega-transform affects mantle upwelling and melting along the SWIR.
- To obtain data on along-axis geochemical variability and temporal variations.
- To examine if the cold thick lithosphere alone controls the history of mega-transforms or do small oscillations of the pole of rotation need to be considered.
- To develop a numerical model that incorporates both the rheology and the stress regime to explain the tectonic structure and to attempt to apply it to the continental transforms.

The activities and initial results of the research cruise S23-AB06 in the Andrew Bain aboard GIN's *R/V Strakhov* are presented hereinafter. During the survey, multibeam bathymetry, magnetics, gravity, SBP, reflection seismic, dredging, were carried out. Other activities, e.g. CTD and SVP casts, and METEO measurements were performed regularly on the way or when dictated by the geophysical acquisition. *R/V Strakhov* sailed from Capetown 2006-02-10, 12:00 local time. At the end of the cruise, the ship docked in Capetown March 10, 2006 at 12:00 local time.

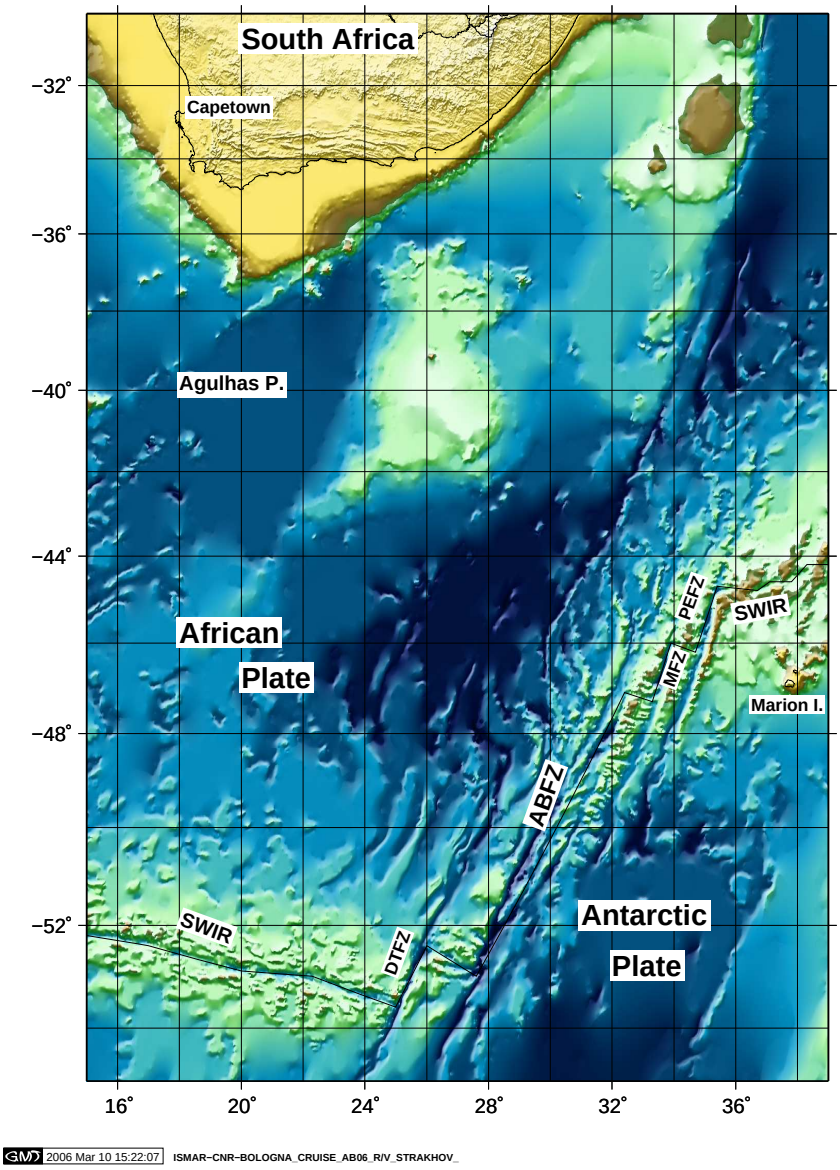

Figure 1: Geographical area setting. Bathymetry and topography from [GEBCO (2003)].

2 GEOLOGICAL SETTING

Oceanic transform boundaries lie on small circles defined by Eulerian POR and are manifested by narrow (a few km) strike-slip deformation zones offsetting two mid-ocean ridge segments [Wilson (1965), Fox and Gallo(1984)]. This is in contrast with continental strike slip deformation zones, such as the the San Andreas or the North Anatolian faults, defined by broad (>100 km), and very complex areas of deformation. The idea of simple, narrow, oceanic transform faults has found some exceptions in a few transforms with very large (>30 my) age offset [Ligi et al.(2002)]. The main example is the Romanche transform, that offsets the MAR in the equatorial Atlantic by over 900 km, with an age offset of ˜50 my. Geophysical and petrological studies have shown that the Romanche has a lens-shaped, >120 km wide zone of deformation between the two ridge axis, with multiple strike slip faults as well as oblique structures; moreover, the basaltic crust is nearly absent within and close to the transform [Bonatti et al.(2001)]. Thus, the Romanche transform system has features similar to the large continental strike slip systems. Numerical models, based on thin viscous sheet, predict fault length to width ratios ranging from 5 to 10 for continental strik-slip zones [England et al.(1985)]. The

Romanche transform has a ratio within the range of continental rather than oceanic transform zones [Ligi et al.(2002)]. Along this extra long, slow-slipping mega-transform, relative motion involves the deformation of extraordinarily thick and cold lithosphere A model that explains the complexities of the Romanche mega-transform has been proposed by [Ligi et al.(2002)]: megatransforms with very large age offset, affecting cold thick lithosphere, are unable to accomodate strike slip motion in a narrow single boundary. These authors analyzed the geometry and the evolution of lithosphere-dominated slow-slipping trasform faults employing a three-dimensional code to simulate mantle flow and thermal state beneath spreading ridges and a two-dimensional finite element code to model deformation of materials with complex visco-elastic brittle rheology. Results of the modelling suggest that the extreme thickness of the lithosphere, hence its rheology, is the most important factor in determining the unusual width and the complex geometry of mega-transforms. [Ligi et al.(2002)] constructed a numerical model to test how lithospheric thickness affects the geometry of an oceanic tranform boundary; they found that long-offset (900 Km) faults produce two major symmetrical faults joining the two ridge segments, with a lens-shaped area between, as observed around the Romanche Fracture Zone.

Another megatransform that may have features similar to those of the Romanche is the Andrew Bain transform, that offsets the SWIR by about 750 km and constitutes a portion of the boundary of the Antarctic Plate. Given the ultraslow spreading rate of the two plates adjacent to the transform, the slip rate is very small (16 mm/yr), and the age offset is rougly 50 million years. Andrew Bain is the longest of a set of close-spaced transforms that includes Du Toit on the south-western side, Marion and Prince Edwards on the north-eastern side

The Andrew Bain Transform is not well known, in part because it is located in a remote and quite inhospitable part of the ocean. It has been partly mapped [Grindlay et al.(1996), Sclater et al.(2005)] and has been sampled at only two sites [Fisher and Goodwillie(1997)]. Topography and satellite gravity derived maps show a broad, multifault, complex zone of deformation; present day seismicity is concentrated on a single linear structure. Oblique *en echelon* structures of unclear origin characterize the central part of the transform domain. [Sclater et al.(2005)] give a synthesis of the complexities of this transform, partly explained by a series of transtensional events resulting from past changes in the ridge/transform geometry.

The objective of the S23-AB06 cruise is therefore to have a better knowledge of this transform, in order to explain its complexities and to test [Ligi et al.(2002)] model.

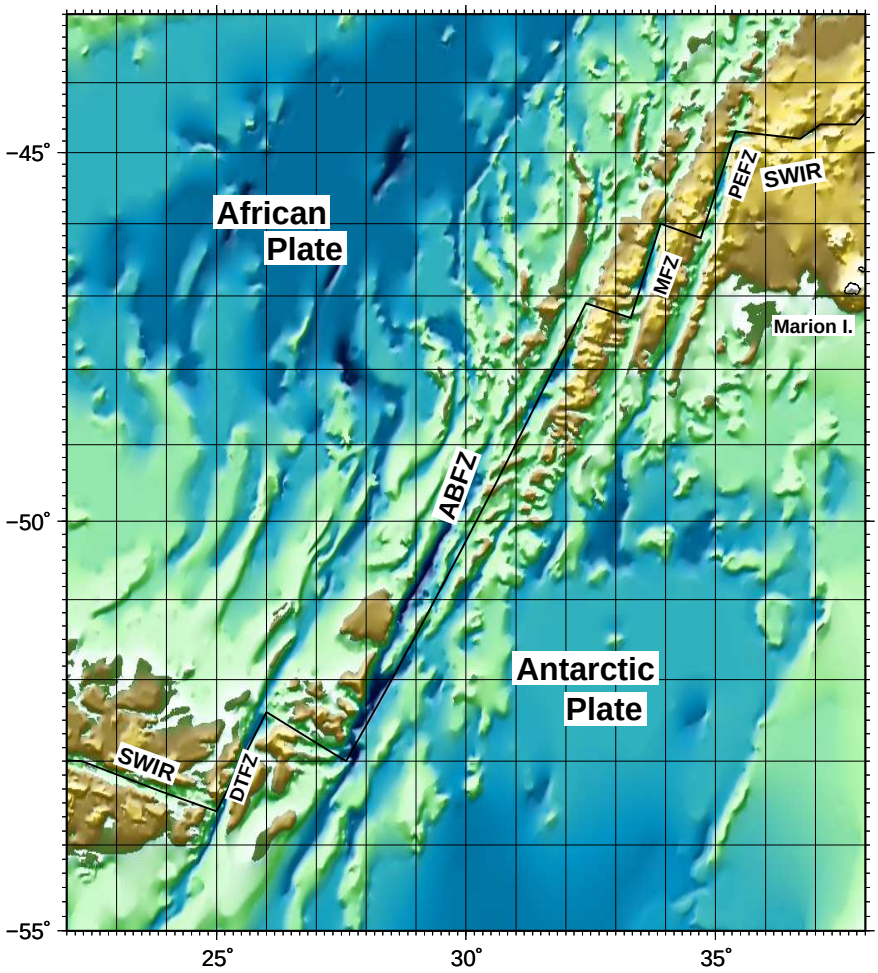

Figure 2: Geographical area setting, Andrew Bain FZ. Bathymetry and Topography from [GEBCO (2003)].

3 CRUISE SUMMARY

SHIP: *R/V Strakhov*
START: 2006-02-10 PORT: CAPETOWN
END: 2006-03-10 PORT: CAPETOWN
SEA/OCEAN: INDIAN OCEAN
LIMITS: NORTH -38:00.0 SOUTH: -53:00.0 WEST: 33:00.0 EAST: 24.0
OBJECTIVE: MORPHOBATHYMETRIC, GEOPHYSICAL AND GEOLOGICAL
OCEANOGRAPHICAL INVESTIGATIONS IN THE ANDREW BAIN F.Z.
COORDINATING BODIES: ISMAR-CNR BOLOGNA (ITALY)
PROJECT RESPONSIBLES: Marco Ligi (ISMAR) Alexander Peyve (GIN)
CONTACT: marco.ligi@ismar.cnr.it
CHIEF OF EXPEDITION: Sergey Skolotnev (GIN)
DISCIPLINES: MORPHOBATHYMETRY, MAGNETICS, GRAVITY, SBP, MCS, DREDGING
WORK DONE: 35000 KM^2 SURVEY+13000 KM^2 TRANSIT MBES,
2500 KM MAGNETICS/GRAVITY, 3800 KM SBP, 245 KM MCS
15 DREDGES, 3 CTD CASTS, 2 SVP CASTS
LOCALIZATION:

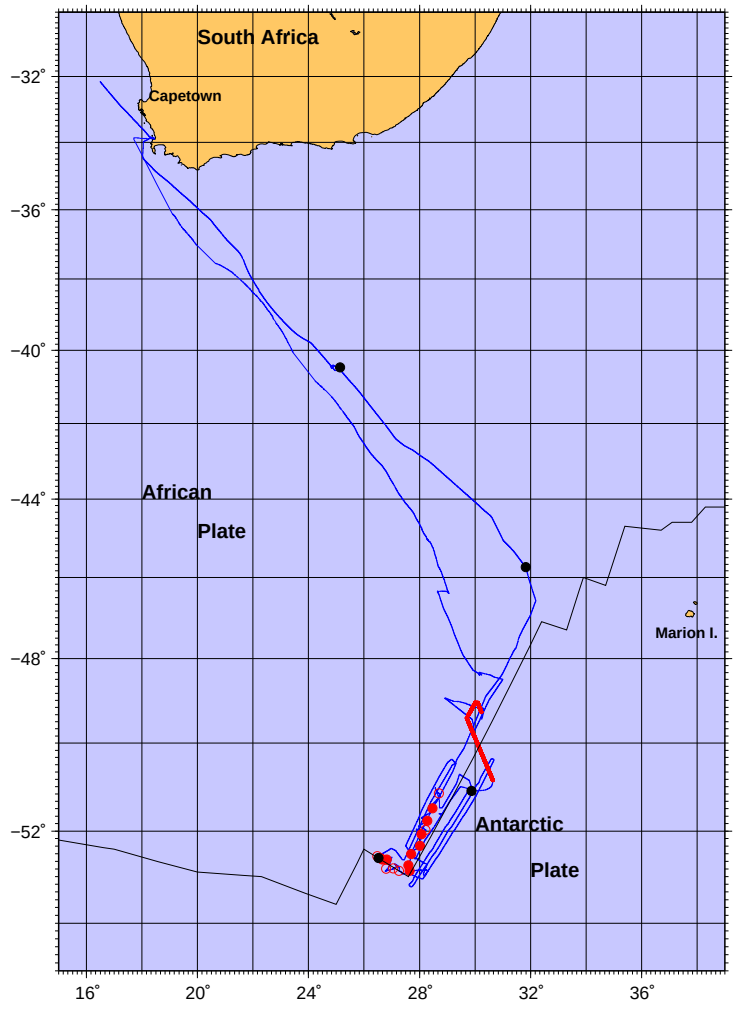

Figure 3: Ship's track during Cruise AB06.

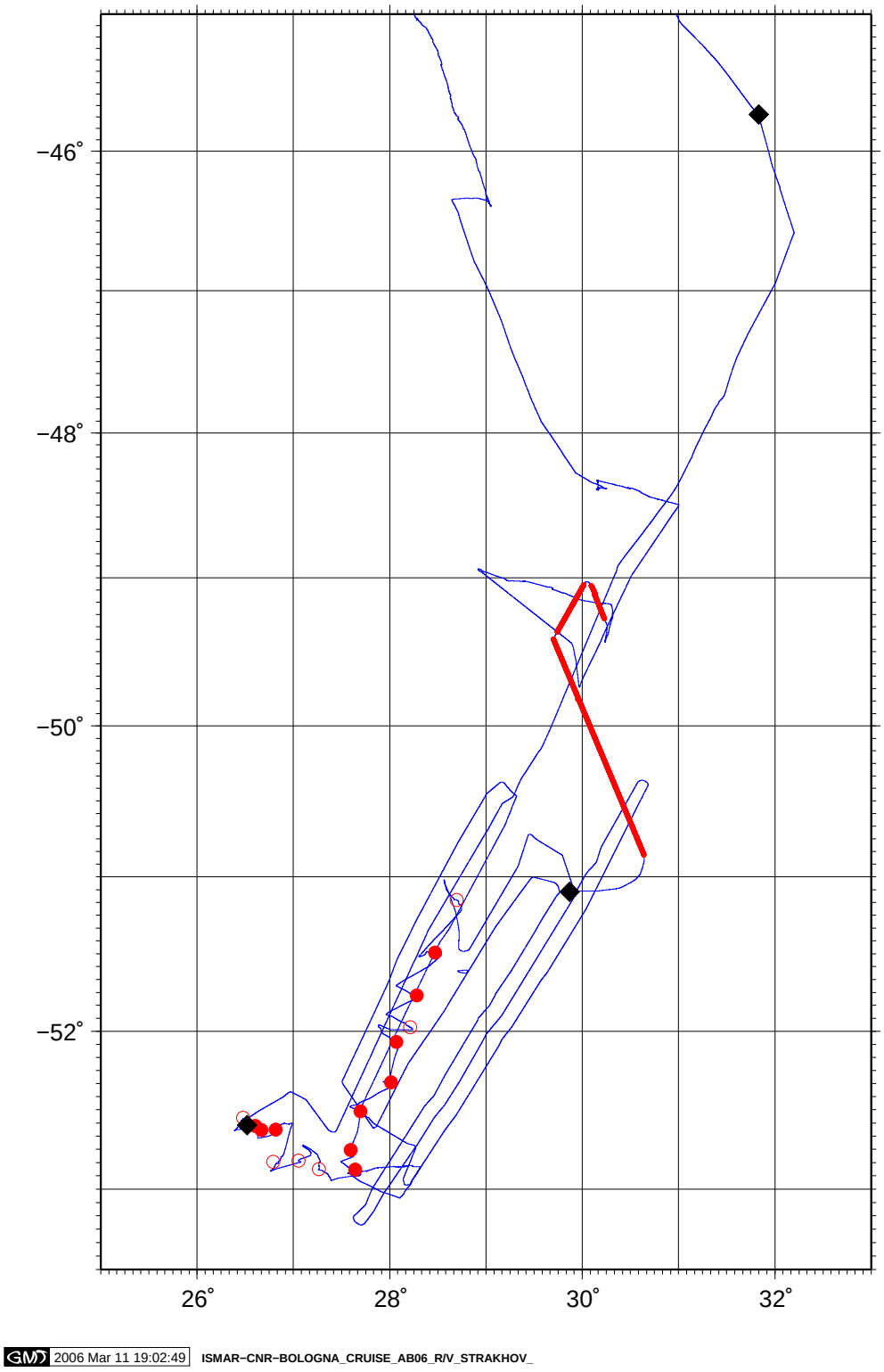

Figure 4: Ship's track during Cruise AB06. Blue: navigation total; red:MCS; red circles: dredging stations (filled when non empty or lost); black diamonds: SVP stations.

SCIENTIFIC AND TECHNICAL PARTIES

PARTICIPANTS	ORGANIZATION	EXPERTISE	tel & email & www
Ligi Marco	ISMAR	Mar.geol.geophysicist	M.Ligi@ismar.cnr.it
Bonatti Enrico	ISMAR, UNIROMA, LDEO		E.Bonatti@ismar.cnr.it
Bortoluzzi Giovanni	ISMAR	Technician	G.Bortoluzzi@ismar.cnr.it
Brunelli Daniele	ISMAR, CEA	Petrologist	D.Brunelli@ismar.cnr.it
Cipriani Anna	ISMAR, LDEO	Petrologist	anka@ldeo.columbia.edu
Zaffagnini Fabio	ISMAR	Geologist	F.Zaffagnini@ismar.cnr.it
Muccini Filippo	INGV	Geophysicist	filippomuccini@hotmail.com
Paganelli Emanuele	Univ.Modena	Student	rotor7876@supereva.it
Mercuri Rosaria	Univ.Roma	Student	mercurirosaria@lycos.com
Sclater John	SIO-UCSD	Mar.geol.geophysicist	jsclater@ucsd.edu
Grindlay Nancy R.	UNCW	Mar.geol.geophysicist	grindlayn@uncw.edu
Takeuchi Chris	SIO-UCSD	Student	ctakeuch@ucsd.edu
Skolotnev Sergey	GIN	Chief of Expedition	skol@ginras.ru
Peyve Aleksandr	GIN	Marine Geologist	peyve@ginras.ru
Turko Natalia	GIN	geomorphologist	turko@ginras.ru
Tsukanov Nikolay	SIO	Marine Geologist	paleogeo@sio.rssi.ru
Persev Aleksey	IGEM	Petrologist	
Eskin Artem	GIN	petrologist	artye@yandex.ru
Chamov Nikolay	GIN	Structural Geologist	nchamov@yandex.ru
Semenov Victor	NSTU	technician	
Yefimov Vladimir	GIN	geophysicist	efimov@ginras.ru
Erofeev Sergey	NSTU	technician	
Rastorgyev Vladimir	GIN	technician	
Baramykov Yury	GIN	geomorphologist	
Kolodyazhnyy Sergey	GIN	Structural Geologist	kolod@ginras.ru
Zotov Leonid	GIN	geophysicist	tempus@sai.msu.ru

Table 2: Scientific and Technical Parties

DIARY OF OPERATIONS

4 MATERIALS AND METHODS

The research cruise was carried out by the 75 meter*R/V Strakhov* (Fig.5), owned and operated by GIN-RAS of Moscow.

R/V Strakhov is used for geological and geophysical work in the World Ocean, and it is equipped with DGPS positioning system, single-beam and multi-beam bathymetry and integrated geophysical and oceanographical data acquisition systems, including CHIRP SBP and other sonar equipment.

The survey was planned to carry out the following tasks

- MBES with a high-resolution multibeam, capable of investigating the sea bottom down to depths of 8000m, alongwith Speed of sound measurements either by CTD or SV probes,
- Magnetometric and gravity investigations,
- SBP investigations,
- Multichannel and single channel reflection Seismic item Dredging and sediment sampling (core and grab)

In addition to these main operational activities, routine on-the-way measurements (meteo, surface C/T, etc) were acquired.

Figure 5: *R/V Strakhov* .

4.1 NAVIGATION AND DATA ACQUISITION

The vessel is set-up for data acquisition and navigation with RESON PDS-2000 software.

Two workstations were used for multibeam data acquisition and QC, interfacing by a multiserial and Ethernet link a RESON 8150 81P processor, an IXEA Octans MRU and gyrocompass, and a Trimble DGPS receiver. Other computers logged magnetics, SBP, meteorological station, conductivity/temperature sensors at the keel, dredging cable tension and the DGPS receiver.

The datum WGS84 and the Direct Mercator projection on 48S were chosen for navigation and display purposes. Timing was set to UTC (some problems occured with the PDS2000 WS set to accomodate the daylight saving time automatically).

A Marine Magnetics SeaSpy Magnetometer tow fish was towed 210m astern, on the port side.

For Multichannel survey a GI-GUN tuned array seismic source was towed 15 m astern, and the first active section of the 48 Ch. seismic streamer was towed 106.5m from the array.

A full-speed, air-gun single channel reflection seismic system was towed on the starboard side.

The instrumental offsets are presented in Fig. 6 and in Tab. 3.

POSITION	ACROSS	ALONG	HEIGHT
VESSEL	0.0	0.0	0.0
OCTANS (GYRO-MRU)	0.0	0.0	0.0
MB 8150	+1.60	+6.62	-5.46
ANTENNA (POS 1)	+0.97	+5.70	+19.58
GRAVIMETER	0.0	5.0	0.0
ANTENNA (POS 2)	+2.0	-23.0	+10.0
GI-GUN ARRAY	-1.0	-65.0	-6.0
FIRST ACTIVE 48CH	6.0	-171.5	-9.0
MAG	-7.00	-243.0	-5.0

Table 3: Instrumental Offsets on Ship Strakhov. Point 0,0 is located in the Computer Room. The main GPS antenna (primary positioning system) is located on point POS1.

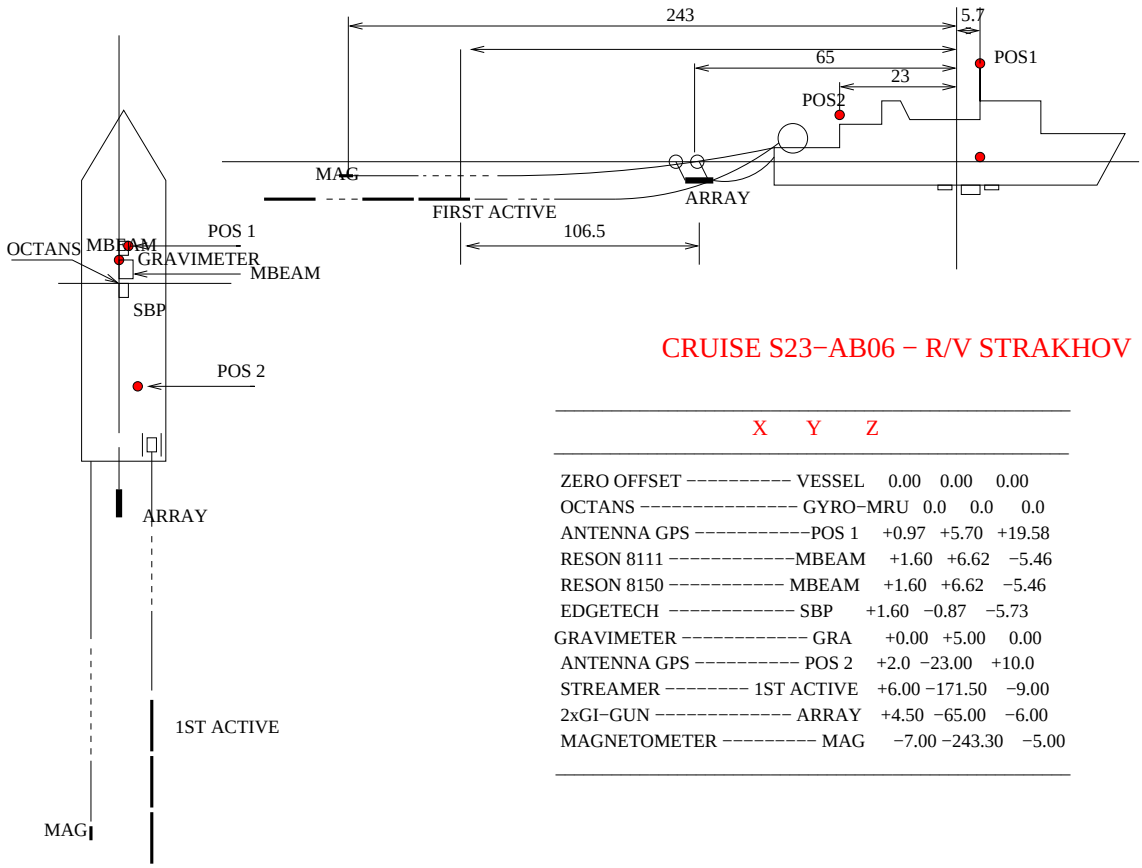

Figure 6: Cruise AB06. Instrumental Offsets on *R/V Strakhov*

4.2 MULTIBEAM BATHYMETRY AND BACKSCATTER

The MBES was the 12 kHz, 234 2° beams, 150°aperture RESON 8150, capable of acquiring data at full ocean depth. The sonar data were collected and recorded in realtime on HD by direct interfacing of the sonar processor 81P to the PDS-2000 software. Two data sets were generated and stored on separate computer for backup on HD and CD/DVD. The PDS-2000 software was able to build a 130 m DTM during the acquisition of the entire surveyed area. The data of cruise KN145-L16 [Grindlay et al.(1998)] were downloaded from the Ocean Ridge Multibeam Database at LDEO as netcdf GMT grids. The data (see Fig.7) were converted from geographical latitude and longitude coordinates to the Direct Mercator 48S projection, and a PDS-2000 DTM was generated and input to the acquisition workstation. The coverage was used for filling gaps and for extending the KN145-L16 survey westward and eastward . Once in the working area and after the extensive test for calibration,

it was found that the KN145-L16 and the newly acquired datasets had no significant misalignments or offsets in the overlapping areas. The two multibeam datasets will therefore be used for an up-to-date regional bathymetric compilation. Backscatter data were recorded in the XTF format and will be processed post-cruise.

A suite of real-time data were collected during the survey, including the Simrad-like format (multibeam) and XTF (reflectivity data). The Simrad-like files were used for extensive post-processing with the MB-System [Caress and Chayes (2004)], PDS-2000 and Kongsberg-Simrad's Neptune.

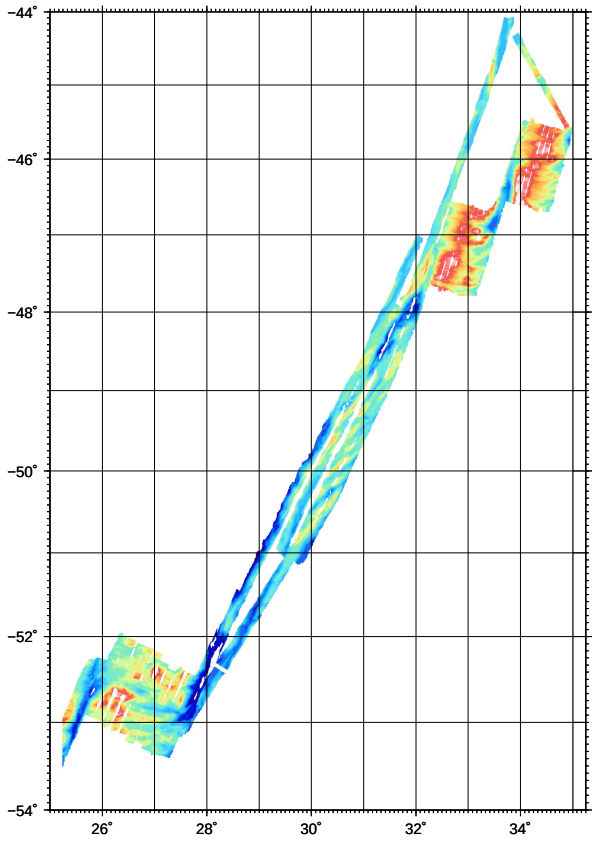

Figure 7: Cruise KN145-L16 Seabeam multibeam grids. Data from the ORMSP database at LDEO.

CALIBRATION

The MBES was calibrated in the Atlantic Ocean during the previous cruise. On the way to the northern end of the ABFZ, on the Agulhas Plateau, we collected data for roll, pitch and yaw calibration (see Fig.8).

The ofssets resulting fron the calibration are presented in Table 4. Several lines were acquired during the survey that will be used as further calibration control.

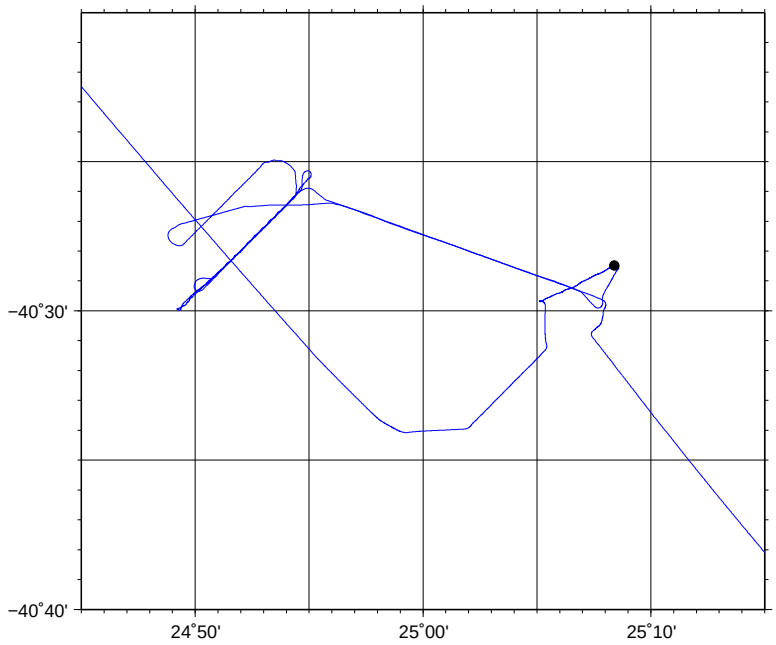

Figure 8: Cruise AB06. Multibeam 8150 calibration dataset.

8150	AB06
roll offset	+0.193°
pitch offset	-0.085°
heading offset	-0.76°
time delay	0.0 s

Table 4: RESON 8150 Multibeam calibration results.

4.3 SOUND VELOCITY DATA

CTD/SVP casts were taken for sound velocity from different sites.

Two probes were used, a RESON Mod. XXX Direct measuring device and the Valeport Model. XXX which gives the direct measurement of SV other than many parameters, including salinity (conductivity) and temperature, that provide another value for SV using well known formulae (i.e. Chen and Millero, UNESCO).

The position of the CTD and SVPstations are shown in Fig. 4, and are reported in Table 5.

ID	DATE	LON	LAT
SVP-01			
CTD-02	2006-02-14	31:49.88	-45:44.13
CTD-03	2006-02-17	26:31.06	-52:35.83
CTD-04			

Table 5: SVP and CTD Stations.

A RESON Mod.SVP 70 direct measuring probe located in the proximity and flush with the multibeam sonar heads provided the necessary real time data for beam forming and detection on the sonar Processors. The probe failed to work on 2006-03-07.

The Sound Velocity profiles were used for real-time acquisition and post-processing.

4.3.1 Modeling of SV synthetic profiles along a track

Two CTD stations were collected data along the >850Km line run westwardly parallel to the ABFZ. The SVP data of first one (CTD02, 2006-02-14) were processed, converted to ASCII, integrated

with the Levitus Database (MB-System, routine mblevitus), imported into the PDS-2000 navigation system.

When the ship arrived at the southern RTI another Valeport CTD (CTD03, 2006-02-14) station was taken, the data processed as above, and input into the PDS-2000.

To be able to process the 850km line from CTD02 to CTD03 we had to prepare synthetic SV profiles along the line, to obtain a smooth transition between the two points of the segment.

Uisng the Levitus Database in MB-System and the two CTD profiles down to 2000m we generated profiles named 1 to 9 (10 intervals of 80km) for input to the PDS-2000. The data were filtered and resampled with GMT's `filter1d` and `sample1d` routines. In the Appendix the scripts are explained in detail.

Figure 9 presents the modeled and measured SVP data .

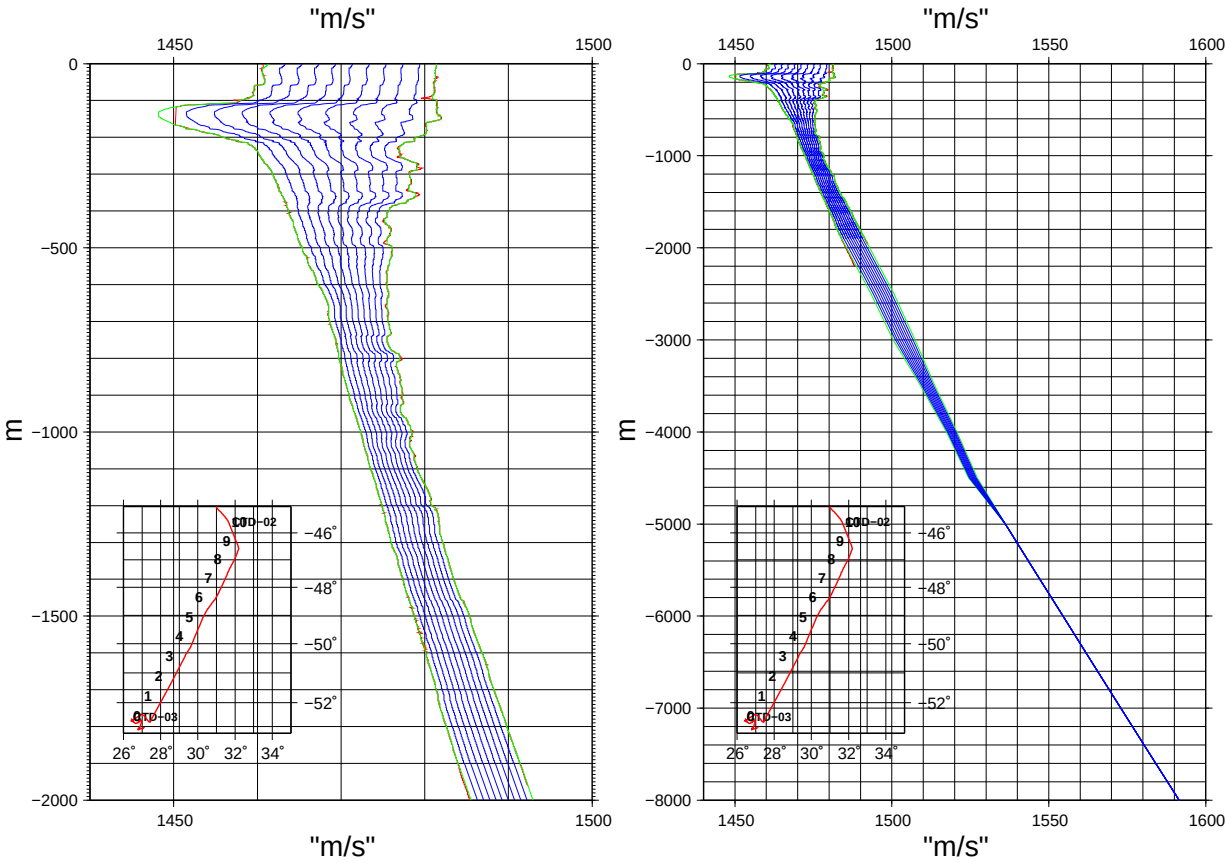

Figure 9: SVP data. Red line: the two CTD stations, CTD03 at left; blue lines: the interpolated lines).

All the PDS data files were therefore replayed according to the position along the transform, producing more accurate PDS-2000 and Simrad-like files.

4.4 MAGNETICS

The Marine Magnetics SeaSpy magnetometer was used. The towfish was kept 210 m off the stern, on the port side. The data was collected by the Marine Magnetics SeaLink software on the multibeam and transit lines,

The software integrated positional data by the NMEA GGA and ZDA strings delivered by two Trimble GPS receivers. From start to 2006-02-27T15:51:00 the ISMAR's receiver (POS2) was used, being directly connected to the magnetometer transceiver. After that timestamp the POS1 ship's GPS data were used, being run to the stern geophysical lab from the data distribution panel in the Acquisition room by using the ship's existing coaxial cable network. The whole sample will be repositioned on the POS1 data by checking magnetometer time with the 1 sec resolution positional data made available on one of the ship's server. The measured time offsets between GPS and Magnetometer

clocks were applied. They were found to vary from -5/-6 sec when using the POS2 receiver (except the very first day of operation, when it was rougly 30 s), to -0.5/-1 sec when using the POS1 receiver.

Figure 10 shows the acquired lines. Intersecting lines will be used to check and minimize day/night variations wherever possible.

The following data processing steps were applied:

- extraction of the navigation and total field ASCII data from the SeaLink data files
- polar transport (GPS antenna offset, angle (hdg-180)) to get the towfish position
- application of the IGRF 2010 (IAGA) to every point, to obtain anomalies
- production of time and wiggle profiles for QC and analysis.

The data of cruise KN145-L16 were provided as field data and were reprocessed with IGRF 2010 coefficients, thus achieving data consistency between the two datasets.

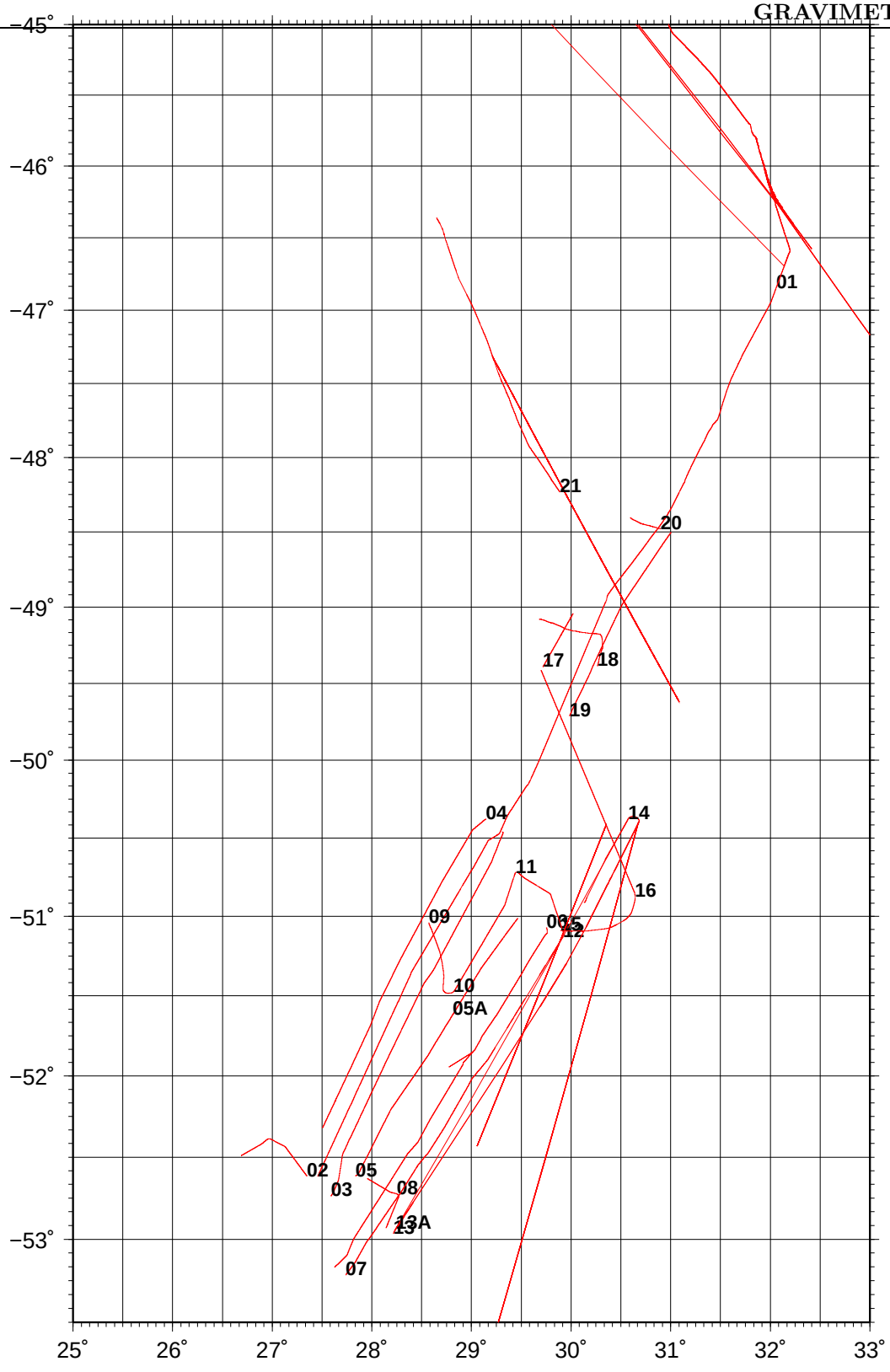

Figure 10: Pattern of acquired magnetic lines.

4.5 GRAVIMETRY

At least two (one in emergency during storms) of a set of 4 quartz thermally stabilized MOD. GMN-K gravimeters assembled in Russia by VNIIgeofisika were running during multibeam lines on medium or long range transits. The sensors were mounted on gyroscopic platforms at the sea level very close to

ship's center of gravity (Tab.3). The instruments have a resolution of 0.04 mGal with an accuracy of 0.2 mgal. Damping by viscous siliceous-organic liquid is used to filter high frequency vertical accelerations. The gravimeter is a-static, having an elastic back connection, and the measuring principle is based on the return-to-horizontal of the system lever actuated by (a) detecting the movement by photoresistors, and (b) turning of the screw connected to the spring. The position of the screw is measured by two voltmeters, digitized and processed by PC every 15 sec during normal survey and every 30 sec during low speed survey, e.g. during dredging. Four gyroscopes connected in pairs along the diagonal, increase the moment of inertia of the pendulum platform, keeping it horizontal within few arcminutes.

The averages of two front-positioned instruments, were used to minimize cross-coupling. Drift of zero point was calculated from the on-board and portable measurements at the berth (see Tab.6). No station in anchor was performed. A few tie lines were run on the predominantly SW-NE multibeam acquisition pattern.

Filtered GPS positions, speed and course over the ground were used to calculate the Eötvös correction. A corrective smoothing procedure[Panteleev (1983)] was used to avoid time-delays and smooth the data. The methematical details can be found in the Appendix 7.1). This procedure can be used in place of the regularization technique. The filter can be built if the model of gravimeter as a dynamical system and the frequency characteristics of the desired signal are known. A first-order model with time constant of 300 sec and a low-pass filter with 1 Hz cut-off frequency were used.

Free-air gravity anomalies were obtained by removal of the GRF80 normal field [Moritz (1984), Torge (1989)], subtracting to the observed values the normal field and applying the Eötvös corrections.

DATE	SITE	SHIP
2006-02-10	Capetown	
2006-03-12	Capetown	

Table 6: Gravimeter drift measurement.

4.6 SEABED SAMPLING

The sea bottom samples were taken by GIN-RAS and ISMAR cylindrical dredges, (Fig.11). Rocks collected by dredging were described on board, logged, sub-sampled and stored away as archive and working samples. Some rocks were cut and polished for further analyses (thin-sections, microscopic observations, etc.).

A total of 15 stations were occupied (see Fig.24 and Table 7).

Figure 11: Dredges.

ID	DATE-START	LON-S	LAT-S	D-S	DATE-END	LON-E	LAT-E	D-E
		dd:mm	dd:mm	m		dd:mm	dd:mm	m
S2315	2006-02-17T08:06	26:28.60	-52:33.08	4364	2006-02-17T11:39	26:28.44	-52:34.96	3612
S2317	2006-02-17T14:59	26:36.17	-52:36.17	2480	2006-02-17T17:53	26:25.07	-52:36.32	2300
S2318	2006-02-17T21:56	26:40.02	-52:37.75	4569	2006-02-17T22:57	26:38.75	-52:38.75	3950
S2319	2006-02-18T01:54	26:49.08	-52:37.50	4769	2006-02-18T04:27	26:51.96	-52:35.61	3865
S2320	2006-02-18T06:56	26:47.52	-52:49.77	4720	2006-02-18T10:18	26:47.52	-52:52.21	3669
S2321	2006-02-18T14:01	27:03.27	-52:49.21	4625	2006-02-18T16:23	27:10.91	-52:46.53	3551
S2322	2006-02-18T21:38	27:15.80	-52:52.49	4805	2006-02-19T00:31	27:21.77	-52:54.88	4034
S2323	2006-02-19T04:30	27:38.51	-52:52.59	6023	2006-02-19T08:19	27:31.90	-52:50.60	4750
S2324	2006-02-19T11:30	27:35.69	-52:45.28	4654	2006-02-19T13:34	27:33.53	-52:44.54	3300
S2325	2006-02-22T17:15	27:41.78	-52:30.48	4112	2006-02-23T00:27	27:39.66	-52:30.12	4007
S2326	2006-02-23T05:08	28:00.97	-52:19.50	5968	2006-02-23T09:33	27:56.70	-52:19.45	4720
S2327	2006-02-23T14:10	28:04.12	-52:04.15	5800	2006-02-23T19:38	28:04.94	-52:03.02	5400
S2328	2006-02-23T23:06	28:12.70	-51:58.42	5767	2006-02-24T04:32	28:03.75	-51:55.12	4749
S2329	2006-02-24T09:18	28:16.75	-51:46.11	5490	2006-02-24T15:45	28:15.46	-51:45.77	5120
S2330	2006-02-24T20:08	28:28.20	-51:29.61	5416	2006-02-24T23:55	28:20.34	-51:30.79	3010
S2331	2006-02-24T06:09	28:41.79	-51:09.03	6386	2006-02-24T11:15	28:34.91	-51:03.82	3850

Table 7: AB06 dredge location.

4.7 SUB BOTTOM PROFILING

'CHIRP' SBP data were acquired by a 5x5 hull mounted Edgetech Mod.X-STAR FULL SPECTRUM Sonar profiler, with operating frequencies ranging between 2 and 5 kHz. The pulse length was maintained at 100 ms while the trigger rates varied from 0.1 to 0.2 Hz according to water depth. The signal penetration was up to 120-130 m below the sea floor. The sonar was controlled by the Edgetech's DISCOVER-SUB-BOTTOM V3.30 software. Digital data were recorded in the JSF format on hard disk. The proprietary format will be converted to SEG-Y for processing.

The navigation data was made available to the system at a rate of aproximately 1 Hz.

4.8 SINGLE CHANNEL SEISMIC REFLECTION PROFILES

The single channel reflection seismic system CSP by GIN RAS was used, being composed by:

- Pneumatic acoustic energy source (air gun) (russian patent): PSK-75 (ПСК-75) - 2.
- high-speed air-gun towing system - 2.
- Firing and control of the pneumatic source: BUP-N (БУП-Н) - 2.
- Air delivery and control
- twin air line hose umbilicals - 2.
- Single channel streamer - 1.
- Analog signal conditioning - 1.
- Digital seismic station SNSP2001/MC (СНСЪ001/МЦ) - 2.
- Analog recorder - 1.

PSK-75 air gun

The PSK-75 ([Efimov (1986)], Fig.12) is a configurable volume chamber (125, 250, 500 1000 ml) air gun with 75mm output port. The working pressure can range from 30 to 200 bar, while the air-gun can be deployed unpressurized. The solenoid electrovalves (Fig.13) are driven by 2 to 20 msec long pulses [Efimov and Kilikov (2001), Efimov (1998)] produced by the BUP-N sub-system 14. The power

circuitry is set-up by thyristor devices and the seismic signature can be modified by different lenghts of the pulses.

The design of the towing system is such that its depth is maintained at 4-7 m with ship speeds ranging 8-12 kn, and it can be deployed at full speed by two-three men using winches or capstans.

Figure 12: PSK-75 Air-gun (1000ml volume chamber) assembled with tow-system on deck.

Figure 13: PSK-75 solenoids.

Figure 14: BUP-N instrumental racks. Left (from top): monitor, digitizer SNSP2001/MC1, analog control. Right(from bottom): oscilloscope, solenoid control BUP-4, solenoid control BUP-5, second digitizer SNSP2001/MC-2.

Figure 15: Air distribution panel..

Air delivery and control (fig.15) is such that one or two guns can work with different pressure settins.

To avoid the condensation freezing (survey in high latitudes), original connectors which maintain a constant diameter for air flow and heating of all the air system control were performed.

The seismic streamer

The GIN-RAS single-channel seismic streamer (Fig.16) was used. The technology is described elsewhere in literature [Edgerton (1963), Ewing and Tirey (1961), Linarski (XXXX)]. However, it was modified to allow high speed data acquisition (8-12 kn) and to increase performance by developping an efficient stretch section made-up by a vacuum-filled polyurethane hose.

Figure 16: Single channel streamer.

The streamer consists of the following parts (from dry-end to tail):

- Tow leader. 120m long Model KG3-40-90 three conductor wires (0.008 Ohm/m) within an armored two layers zinc plated steel shield, breaking force: 4000 kg. .
- Impedance matching. Construction: transformer placed between tow leader and stretch section. Coefficient transformation: 0.2. Magnetic material: permalloj. Resistance of primary: 1.1 kOm, resistance of secondary 40 Ohm
- Stretch section. Construction: GIN-RAS. 10 m long vacuum filled polyurethane hose
- Active section. Construction: the receiver antenna is placed within a polychlorvinil hose filled with diesel fuel. Length of hose: 30 m. Outside diameter of hose: 54 mm. Thickness of hose: 5 mm. Trade mark of ceramic: PDS-21. Number ceramic elements: 50 Step of ceramic elements: 0.5 m. Connection of the ceramics: parallel. Length of the antenna: 25 m.
- Tail Section. Length of the hose: 10 m. Outside diameter of the hose: 36 mm. Thickness of the hose: 4 mm.
- Stabilizer. Rope diameter 10 mm. Length: 30 m.
- Connectors.Construction: GIN-RAS. Designed to keep the conductors in a pressurized environment, to provide stronger waterproofness. Number contacts: 3.Pressure on the contact: 600 bar. Pressure of air within the contact zone: 100 bar.

Digital data recording

Digital acquisition (72 db dynamical range, sampling rate 1 kHz, 14 bit DAC, was performed by two (Fig.14) Intel based PC workstations SNSP2001/MC designed by NSTU. The software is able to digitize and write data in the SEG-Y format, while presenting the user the real-time data for control and QC (seismic trace, bottom profile, amlitude spectra etc). Fig.17 gives examples of the data acquisition windows on the workstation.

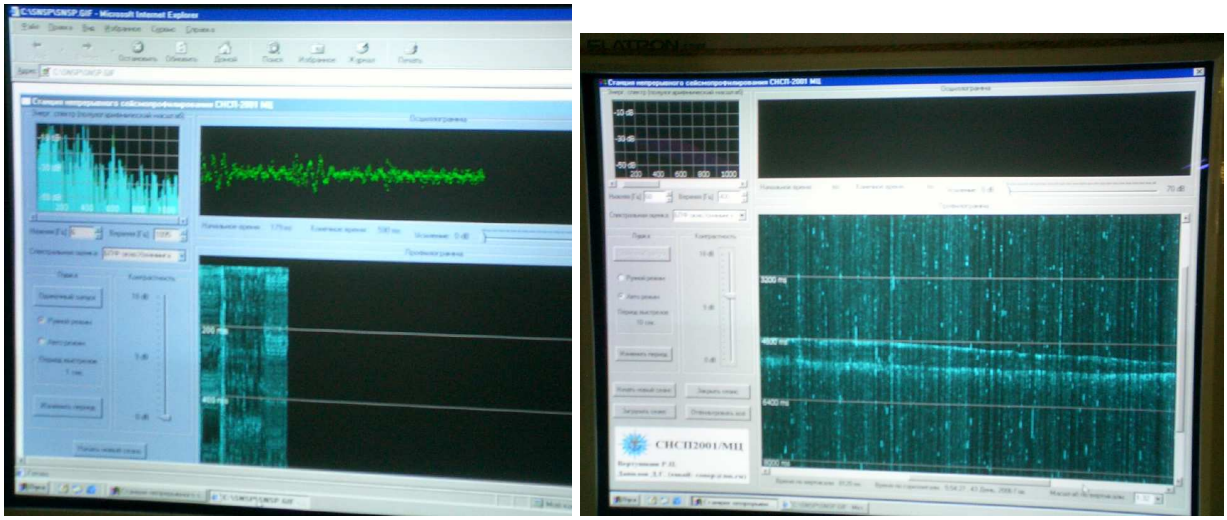

Figure 17: Data Acquisition windows on digitizing workstation.

Main parameters for digital seismic station SNSP2001/MC.

- Gain control.
  - Input for seismic signal: differential or simple.
  - Input signal: >100mV, R-input. >1 MOhm,
  - Maximum gain for seismic signal: 100000.
  - Limit seismic signal level input: <100 V.
- Synchronization.
  - Input/outputs: TTL
  - Output signal DAC level: 1.2 V cut.
- Analog Filtering.
  - Active Butterworth filters of 4-th order.
  - Slope: 45 dB/oct.
  - high-pass 20, 60,120,230,300 Hz;
  - low-pass 400,800,1000,1500,2800 Hz.
- Digital recording
  - 14bit ADC.
  - Conversion frequency up to 8 kHz
  - Format for seismic recorder: SEG-Y.

Main survey CSP specification

- Speed towing range: 8-15 knots.
- Depth of streamer at knots: 7.5 m.
- Sensitivity on 100 Hz: 17 mV/Pa
- Output impedance (40-250 Hz): 1.6 kOhm.
- Frequency range: 10-2000 Hz
- Penetration: to 2 sec in sediments

- Noise level at 10 knots (40-250 Hz) in good sea state:
  - direct signal: 32 dB
  - inputing level: 25 mV
- Resolution 25 m.

Miscellaneous

Analog data are filtered and conditioned by GIN-RAS equipment. The real-time data are then routed to a Raytheon", model LSR-1807M electrostatic paper recorder .

Further information about GIN RAS CSP system can be found at http://atlantic.tv-sign.ru.

4.9 MULTICHANNEL SEISMIC REFLECTION PROFILES

High-resolution multichannel seismic were performed by ISMAR using an array of two synchronized SERCEL (formerly SODERA-SSI) GI-GUN (Fig.18), (in the 105+105 c.i. Harmonic configuration) pneumatic sources, powered by two 2000 L/Min, electrically driven air compressors. The pressure to the gun ranged from 130 to 180 bars, depending on speed of profiling and compressor's delivery. The seismic data were collected by a MOD.29500 TELEDYNE 48 channel streamer (Fig.19), digitized and recorded on DDS-1 and DDS-2 DAT tapes by a OYO-GEOMETRICS's STRATAVISOR seismograph in the SEG-D 8048 Revision.0 format, with sampling rate of 1 msec and record lengths of 12+ secs. The group interval was of 12.5m for a total active length of 600 m. The 100 m tow leader, two 50 m stretch sections and tail rope made up the streamer to a total length of 900 m. The seismic source was fired by IGM's gun-control equipment [Masini and Ligi (1995)] (Fig.19) that introduced a fixed delay of 10 msec from the time break. The injector delay was set around 44 msec $\pm$ 2 msec according to pressure delivered by compressors. The guns were automatically synchronized by adding delays ranging $\pm$ 0.5 msec to the near gun. An additional delay of 15 msec to the above figure had also to be added due to the opening of electrovalve, thus reaching 25 $\pm$ 0.5 msec from the time break. Shot distances were of 50 m, thus achieving coverages of 600%. The time break was provided by the seismic module in the NAVPRO software, with the *DISTANCE FROM PREVIOUS SHOT* setting, in order to maximize the survey flexibility allowing the *SHOT NOW* capability when enroute. The depth of the source ranged between 5 and 7 m depending on sea state. The streamer was kept at 10-12 m depth with SYNTRON RCL-2 cable-levelers, using a Teledyne Mod. 28951 depth control system.

The data were processed onboard using the DISCO/FOCUS packages by PARADIGM, up to the time-migration of some sections, using a standard processing sequence.

An offset of 106.5m between the source and the first active was found by measuring the time distance on the sections, subtracting the 25 msec delay, converting to distance by using value of 1466 m/s.

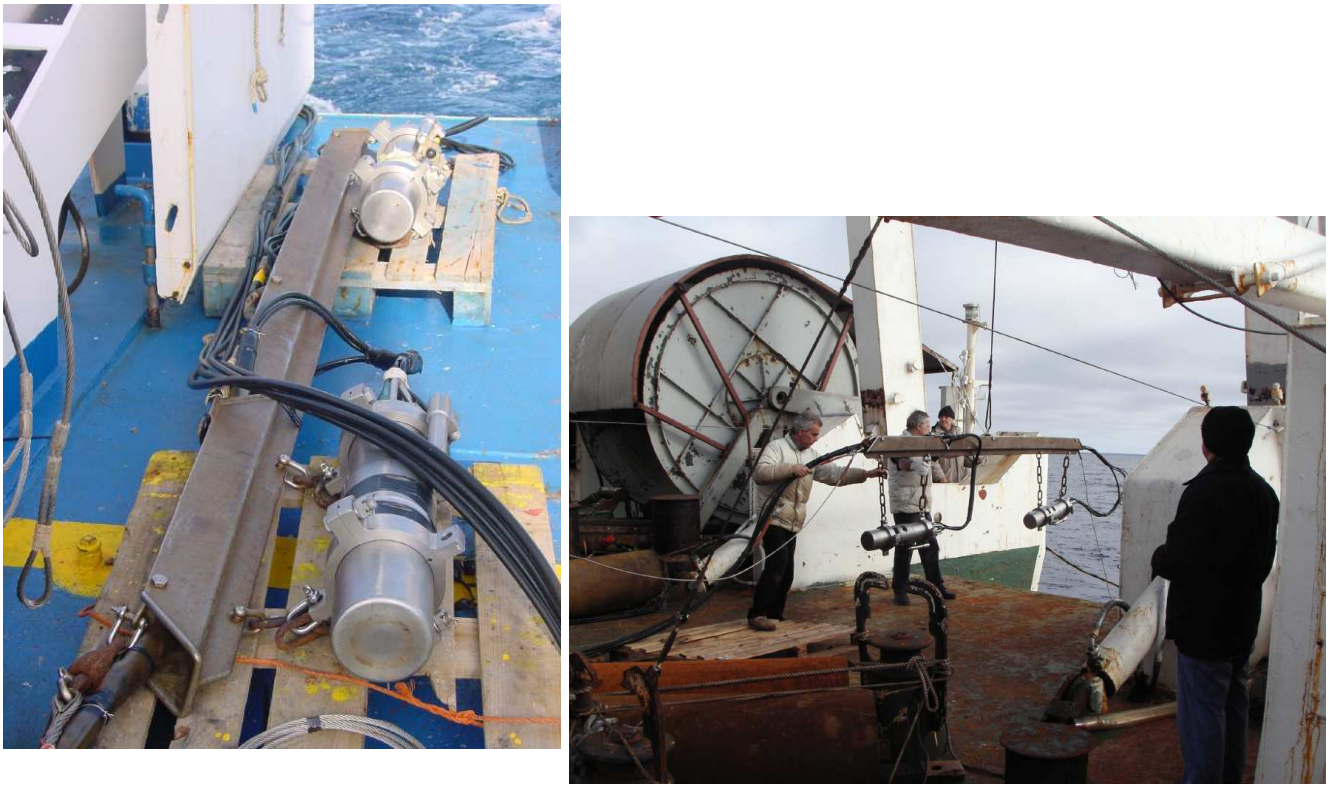

Figure 18: GI-GUN Array.

Figure 19: Left: GI-GUN Array Synchronizer. Center,right: Multichannel streamer on Strakhov's winch.

The runlines can be shown in Fig.20.

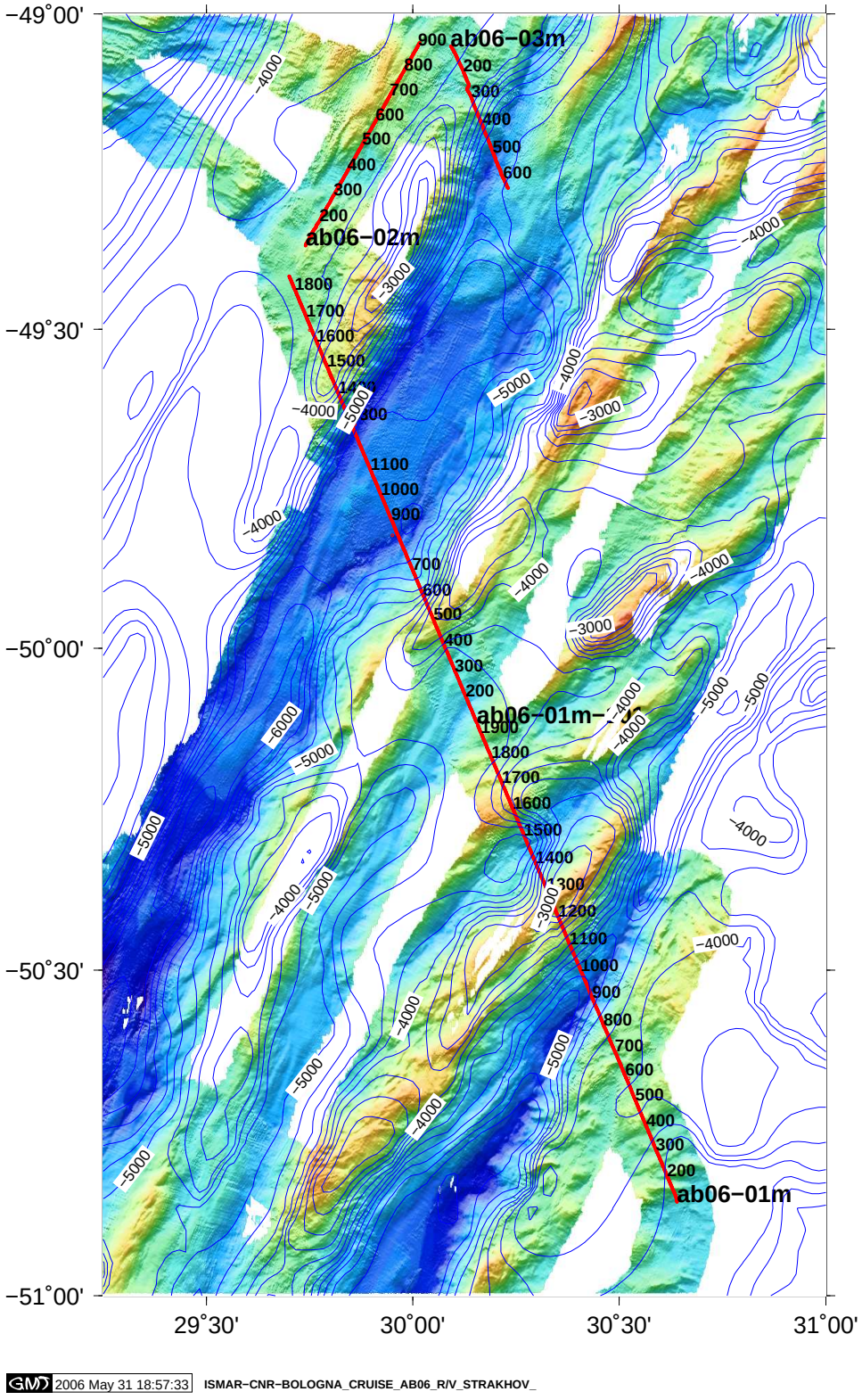

Figure 20: MCS navigation lines.

4.10 MISCELLANEOUS

The datum was set to WGS84 and the Direct Mercator on 48S was chosen for navigation and display, and data acquisition. The time zone was set to the UTC for the whole data acquisition process. The NAVPRO sofwtare was instead set to the UTM 35 for MCS operations.

The positioning maps and bathymetric images were done with GMT [Wessel and Smith (1995)].

Bathymetric data were complemented by the GEBCO data and previous cruises data.

The computing center used three INTEL based PC running the SUSE GNU-Linux and the Microsoft Windows 2000 O.S., and two SUN workstations running Solaris 8, in addition to some portable computer for data acquisition and efficient data processing.

The Linux machines were used as data repositories using the SAMBA software. A WWW server on a Linux machine was used to share ongoing information and results.

Backups were loaded on DAT tapes, DVD and CD-ROM, and shared among the participants.

Photographs were taken by digital video and cameras, and no copyright was given on the published materials.

5 INITIAL RESULTS

Initial results are presented, in order to address the importance of the preliminary findings and processing sequence of the data acquired. As explained in Chapter 4, during the cruise we acquired:

- Multibeam bathymetric and backscatter data, with SVP casts ranging from 0 to 2000 m water depth.
- Magnetometric and gravimetric data
- Multichannel and Single-channel Seismic Reflection profiles
- Sub-bottom profiling
- Rock sampling

5.1 BATHYMETRY

Pattern of the multibeam lines during operation in the study area are presented in Fig.4. A surface area of approximately 35000 km^2 was covered in the survey.. Partial processing of the acquired data by the RESON 8150 was carried-out during the cruise with the Neptune, MB-SYSTEM and PDS-2000 software. The quality of the data acquired varied from good to acceptable, excluding lines run in bad weather conditions because of the rough seas.

The DTM were produced in projection (Direct Mercator and UTM) and geographical domains, with the point clouds of post-processed data, using GMT's and ISMAR routines.

Fig.21 shows a 3-d view of the ABFZ southern RTI.

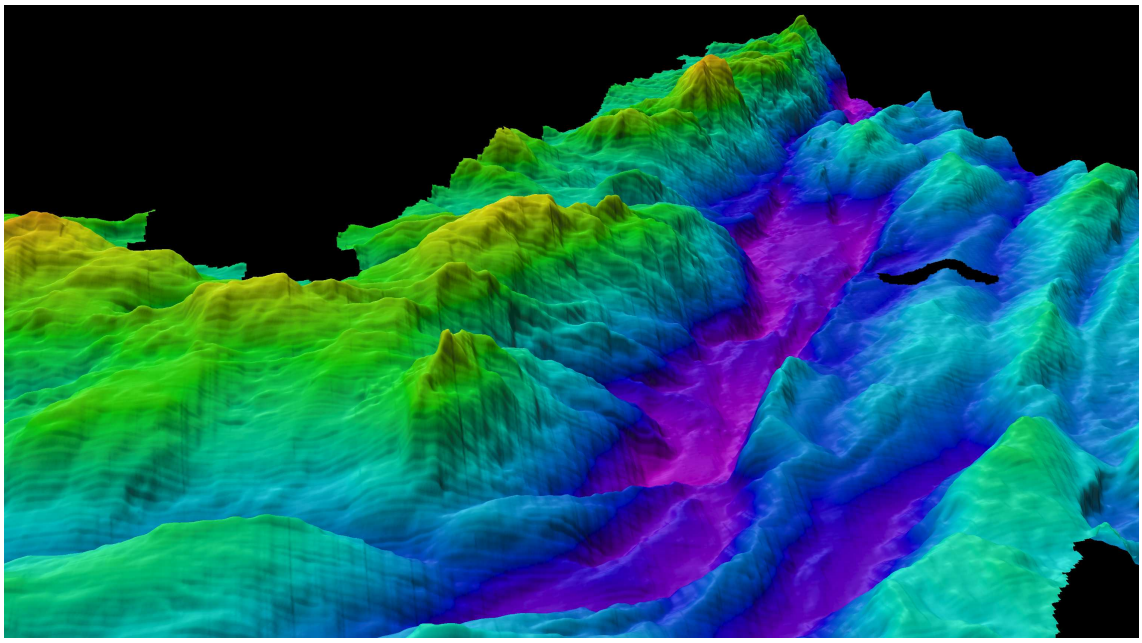

Figure 21: 3D view from SW of the SWIR ABFZ RTI.

5.2 MAGNETICS

The data were processed on board. The IGRF 2010 reduced data ranged from -350 to +350 nT. Further processing will require the analysis of the closest on land observatory data.

The obtained data along the western transverse ridge showed clear magnetic anomalies lineating possibly up to Anomaly 13. No anomalies were present within the transform domain and along the eastern ridge segment between the DTFZ and ABFZ.

Figure 22 shows 18 h of data collected along seismic line AB-01M (Fig.20). The presence of some spikes will be investigated further against observatory data.

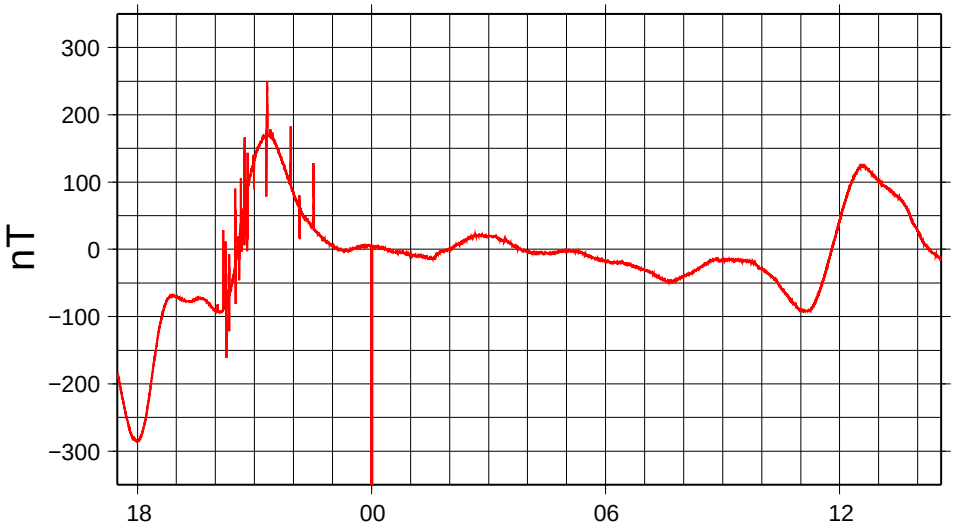

Figure 22: Example of the unfiltered IGRF anomaly data collected along seismic line 01M.

5.3 GRAVIMETRY

Figure 23 shows the gravimetric anomaly and depth along three runline. Despite of instrumental accuracy of 0.2 mgals , we can estimate a true accuracy of the order of several mgals, due to thermal instabilities, storms, non-linear drift of gravimeter because of long period of work.

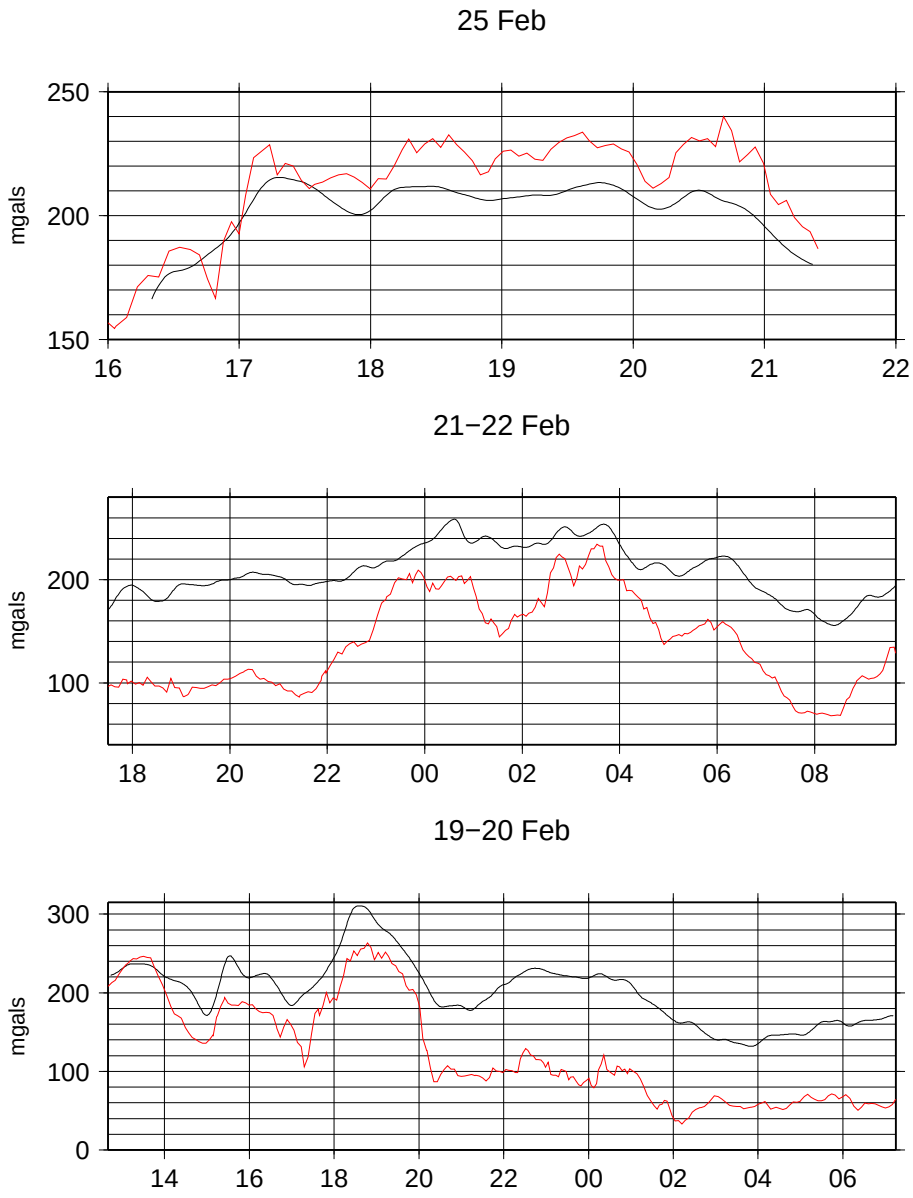

Figure 23: Example of filtered anomaly gravity data collected along some lines. Red lines: bathymetry.

5.4 SEABED SAMPLING

We focused on dredging, with the aim to recover basalts and mantle materials. The location and description of the samples are located in Tab.7.

Fifteen sites were dredged for rock samples from submarine slopes and escarpments in and around the ABFZ (Fig.24. Two dredges were lost during the operations. One dredge sample contained basalts, while all other dredges contained peridotites and/or erratics.

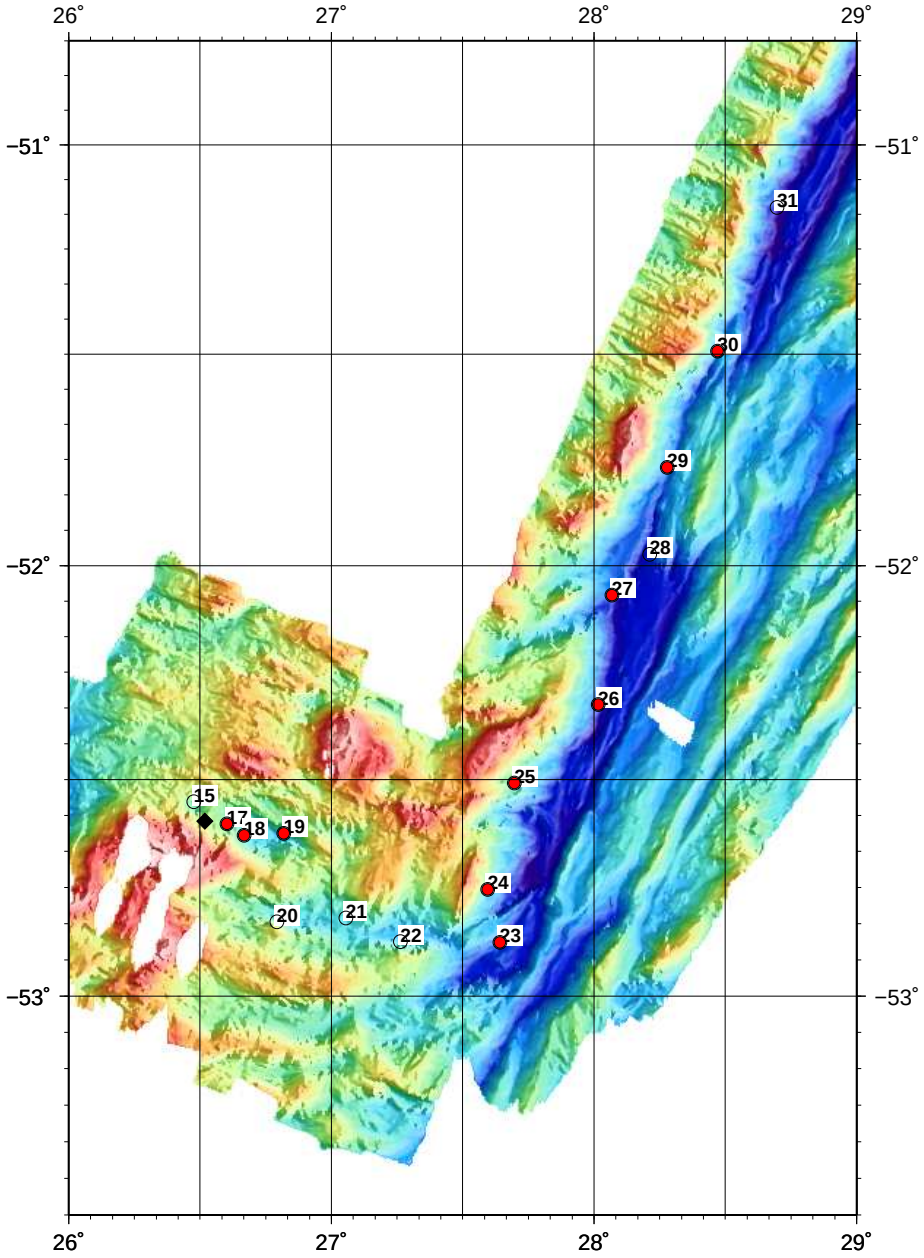

Figure 24: AB06 dredge locations.

The basalts and peridotites will be subjected to intense geochemical (major and trace elements, Nd, Sr, Os and other isotopes, water content, melt inclusions) and geochronological analyses, especially on the glasses of the pillows.

Table 8 gives details on the rock lithology and recovery. In Appendix 7.3 Table 9 presents the rock subsampling and descriptions.

STA-ID	TECTONICS	LOCALIZATION	LITHOLOGY	RECOVERY
S2315	Ridge axis	Near transform fault		lost
S2317	Ridge axis	Western segment; small axial basin	99% pillow basalts with or without fresh glassy crust; 1% gabbros; 1 peridotite sample	100 kg
S2318	Ridge axis	Western segment; Central deep basin	60% peridotite, 40% gabbros, 1 basalt	30 kg
S2319	Ridge axis	Western segment; North steep fault	erratic granitoids	10 kg
S2320	Ridge axis	Eastern segment		empty
S2321	Ridge axis	Eastern segment		empty
S2322	Ridge axis	Eastern segment		empty
S2323	RTI	Nodal basin; west RTI	50% peridotite, 50% erratic granitoids	5 kg
S2324	RTI	Inside corner high; west RTI	100% peridotite	5 kg
S2325	FZ	Western wall FZ	95% peridotite, 5% breccia	100 kg
S2326	FZ	Western wall FZ	80% peridotite, 15% erratic granitoids, 5% basalt	
S2327	FZ	Western wall FZ	erratic granitoids	5 kg
S2328	FZ	Western wall FZ		empty
S2329	FZ	Western wall FZ	1 sample of gabbro (erratic?)	2 kg
S2330	FZ	Western wall FZ	erratic granitoids	15 kg
S2331	FZ	Western wall FZ		empty

Table 8: AB06 dredge descriptions.

5.4.1 Southern ridge axis

The southern ridge axis impacting the Andrew Bain Fracture Zone is formed by two overlapping ridges. Two dredges were carried out in the westernmost of the two overlapping segments. S2318 is located in the small deep western axial basin and S2319 in the central large axial basin. Dredge S2317 is located on the flank of a conic structure which suggests recent volcanic activity. Numerous fragments of pillow basalts have been recovered together with minor gabbros and one mantle peridotite. Basalts belong at least to two different time events. One population of basalts is fresh, covered by thick glassy crust, probably a recent event. The other one appears more altered, coated by Fe-Mn and characterized by a marked vesicularity, probably an older event. Both populations are aphyric, with rare plagioclase feno- or megacrysts. The small Pl-Cpx gabbroic samples show a variable grain size but overall they are strongly altered. One small fragment of granular serpentinized peridotite has been also recovered together with a small fragment of breccia cemented by Fe-Mn mineralization. Dredge S2318 comprises gabbros and mantle peridotites in equal proportions plus minor dunites and breccias. Gabbros have variable grain size from micro to pegmatitic. Compositionally they vary from troctolitic to olivine-bearing gabbro, gabbro, leucogabbro and oxide-bearing gabbro. Mantle peridotites have granular to porphyroclastic to mylonitic textures. They vary from harzburgitic to lherzolitic terms, deeply serpentinized, with strong modal variability in orthopyroxene content. Clinopyroxene grains usually have a marked lineation crosscutting the rock foliation. They are associated with spinel and rarely with plagioclase grains. All peridotites show a weak to well developed high-T foliation marked by opx. Mylonites of both harzburgite and lherzolites terms, are also present. Dunites are completely serpentinized, cut by thin spinel chains. An oficalcitic breccia with dunitic clasts is cemented by carbonatic ooze.

Dredging attempts of the eastern overlapping segment have provided only few erratic samples. This ridge segment is covered by a thick layer of sediments with apparently no recent magmatic activity. Only one peridotitic mylonite has been recovered on the nodal basin wall at the eastern RTI.

5.4.2 Western wall of the transform valley

Seven dredges have been carried out along the western wall of the transform valley of the AB FZ, moving away (northward) from the RTI, i.e. with increasing age. Sampling sites are spaced about 30 km apart each corresponding to roughly 4 My in time. Only the first three dredges recovered samples (S2324, S325 and S2326); one dredge was empty and the farthermost from the RTI recovered only erratic pebbles of possible Antarctic origin. Recovered rocks are mainly granular to porphyroclastic (and less mylonitic) mantle peridotites, modally ranging from harzburgite to lherzolite. These samples show a strong variability in the opx/ol similarly to the peridotites recovered along the ridge axis. They are associated with variable shape of the granular orthopyroxene, ranging from rounded to lobate in the undeformed samples. Plagioclase appears locally scattered in the olivine matrix or along veinlet, sometimes associated with minor clinopyroxene. Several high-T gabbroic intrusions cut the mantle assemblage forming centimetric veins and patches. Gabbroic veins are also present as low-T intrusion along cracks, but they are usually strongly altered. Minor gabbroic and dunitic samples have been recovered together with oficalcitic breccias cemented by carbonate.

5.5 MULTICHANNEL SEISMIC

Due to very bad weather we were able to run only one line crossing the ABFZ. The line AB01M was processed up to the stack and time migration. Fig.25 shows part of the neartrace (channel 22, offset 425 m from source) profile. The valley is filled by sediments which appear to be folded and displaced by strong currents flowing along the two walls.

The data seems to have a good potential also for deeper reflections.

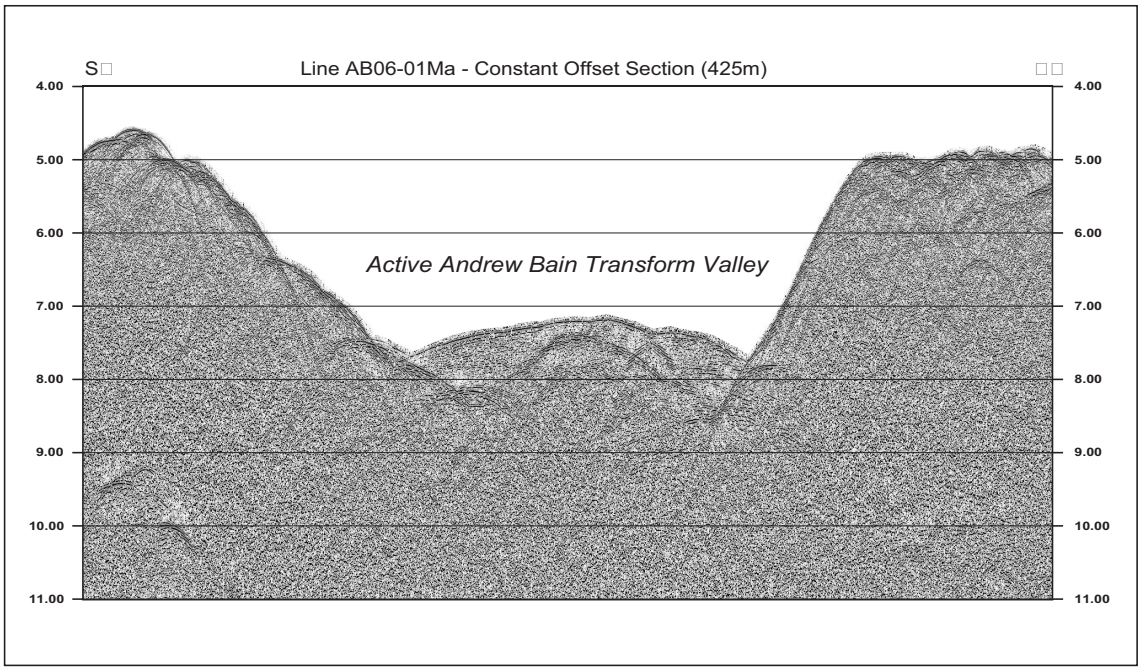

Figure 25: Neartrace profile of line 01Ma.

6 CONCLUSIONS

We have written these conclusions right after the end of the cruise and they are to be considered preliminary.

During S23-AB06 cruise in the Andrew Bain Fracture Zone we obtained:

1 high resolution bathymetric images and DTMs of the area

2 high resolution magnetometric profiles

3 across and along basin multichannel reflection seismic lines

4 bottom samples (dredges)

The data is under detailed processing and analysis, and we expect to have new insights into the Andrew Bain FZ geology and geochemistry.

The major accomplishments were (a) to complete a full multi-beam survey of the southern section of the Andrew Bain transform fault and (b) to dredge in the southern spreading centers and along the south western wall of the transform fault.

In the southern spreading center we found basalts, gabbros and a few ultra mafics on the segment closest to the Du Toit Transform Fault. We tried but did not complete successful dredges within the trough that marks the spreading center segment closest to the Andrew Bain. However at the presumed spreading center/transform fault intersection (SC/TFI) we dredged significant quantities of peridotite with very little to no basalt or gabbro. On the western wall we had a series of successful dredges on successively older crust before we encounter significant sediment and we recovered no more material. The dredges, which started in greater than 6000 m of water depth within the transform valley, recovered almost entirely ultra mafic rocks. We plan to examine the transient nature of the temperature of the intrusion zone with these samples.

Completing the survey of the southern part of the transform permitted us to identify the major transform valley from the SC/TFI north to about 50°S. Clearly it follows the western portion of the transform valley with at least one small offset to the west. With our preliminary understanding of the morphology we do not see how to account for two high angle dip slip events reported by Sclater et al., (2005). Motion along the southern section of the transform domain appears to be taken up by a series of linear offsetting transform faults. This is very different to the complex relay basin type motion observed in the northern section of the domain.

In addition to the work to the southern section of the transform fault we also completed a number of north-south lines both within, and to the west and east of, the transform domain. These lines filled in, and extended to west and east of the domain, our previous survey in the area. We obtained identifiable magnetic lineations on the normal ocean floor created at the southern spreading center. In addition we established the morphological limit of the south eastern extent of the transform domain. A final success was a 48 channel seismic line across the center of the transform domain. This line identified significant thicknesses of sediment within the central transform valley and dipping and truncated reflectors within the en echelon topographic highs that dominate the morphology of the central portion of the domain. These reflectors appear to indicate a tectonic instead of intrusive origin for these features. Unfortunately bad weather prevented the completion of the two additional seismic lines that we had planned. All in all we had much success on this cruise and will be able to modify and extend many of the preliminary conclusions that resulted from the initial survey to the Andrew Bain from R/V Knorr in 1996.

References

[Bonatti et al.(1994)] Bonatti, E., M. Ligi, L. Gasperini, A. Peyve, Y. Raznitzin, and Y. J. Chen , *Transform migration and vertical tectonics at the Romanche Fracture Zone, equatorial Atlantic*, 1994, J. Geophys. Res., 99(B11), 21,779-21,802.

[Bonatti et a.(1996)] Bonatti, E., Ligi, M., Carrara, G., Gasperini, L., Turko, N., Perfiliev S., Peyve, A., and Sciuto, P.F., *Diffuse impact of the Mid-Atlantic Ridge with the Romanche transform: An ultracold ridge/transform intersection*, 1996, Journal of Geophysical Research, 101, 8043-8054.

[Bonatti et al.(2001)] Bonatti, E., Brunelli, D., Fabretti, P., Ligi, M., Asunta Portaro, R., Seyler, M., *Steady-state creation of crust-free lithosphere at cold spots in mid-ocean ridges*, 2001, Geology, 29: 979-982.

[Caress and Chayes (2004)] Caress, D. and Chayes, D., *MB-SYSTEM Release 5*, 2005, URL: www.ldgo.columbia.edu/MB-System.

[Efimov (1986)] Ефимов В.Н., *Сеисмицеский пнеумоизлиыиател. АС-СССР на изобретение Н°144524*, 1986.

[Efimov (1998)] Ефимов В.Н. , 1998, Патент РФ на изобретение Н°2109309.

[Efimov and Kilikov (2001)] Ефимов В.Н. анд Уиликов А.М., , 2001, Патент РФ на изобретение Н°2174241.

[Edgerton (1963)] Edgerton H.E., *Sub-bottom penetrations in Boston Harbour*, 1963, J.Geophys.res., V68, N.9.

[England et al.(1985)] England, P., Houseman, G., and Sonder, L., *Length scales for continental deformation in convergent, divergent, and strike-slip environments: Analytical and approximate solutions for a thin viscous sheet model*, Journal of Geophysical Research, v. 90, p. 3551-3557.

[Ewing and Tirey (1961)] Ewing J.I. and Tirey G.B., *Seismic profiler*, 1961, J.Geophys.Res., V66, N.5.

[Fisher and Goodwillie(1997)] Fisher, R. L., and A. M. Goodwillie, *The physiography of the Southwest Indian Ridge*, 1997, Mar. Geophys. Res., 19(6), 451-455.

[Fox and Gallo(1984)] Fox, P. J., and Gallo, D. G., *A tectonic model for ridge-transform-ridge plate boundaries: Implications for the structure of oceanic lithosphere*, 1984, Tectonophysics, v. 104, p. 205-242.

[Gasperini and Stanghellini(2005)] L.Gasperini, G.Stanghellini, *SEISPRO, a processing software for high resolution seismic data*, 2005, ISMAR Tecnical Report, N. , in preparation.

[GEBCO (2003)] IHO-UNESCO, *General Bathymetric Chart of the Oceans, Digital Edition*, 2003, www.ngdc.noaa.gov/mgg/gebco.

[Grindlay et al.(1996)] Grindlay, N. R., J. A. Madsen, C. Rommevaux-Jestin, J. Sclater, and S. Murphy , *Southwest Indian Ridge 15E-35E: A geophysical investigation of an ultra-slow spreading midocean ridge system*, 1996, InterRidge News, 5,7-12..

[Grindlay et al.(1998)] Grindlay, N. R., J. A. Madsen, C. Rommevaux-Jestin, and J. Sclater, *A different pattern of ridge segmentation and mantle Bouger gravity anomalies along the ultra-slow Southwest Indian Ridge (15:30E to 25E)*, 1998, Earth Planet. Sci. Lett., 161(1-4), 243-253.

[Ligi et al.(2002)] Ligi, M., E. Bonatti, L. Gasperini, and A. N. B. Poliakov *Oceanic broad multifault transform plate boundaries*, 2002, Geology, 30(1),1-14.

[Linarski (XXXX)] Линарский Г.Н., , ШШШШШ, ВИНИТИ Н°832-75 деп.

[Masini and Ligi (1995)] Masini L. and Ligi M., *Sistema di controllo e sincronizzazione cannoni sismici ad aria compressa*, 1995, Rapporto Tecnico IGM N.37, 126pp.

[Moritz (1984)] Moritz H., *Geodetic reference System 1980, The Geodesist Handbook*, 1984, Bull.Geod., 53,388-398.

[Panteleev (1983)] Panteleev V.L., *Foundations of Marine gravimetry*, 1983, Nedra, Moscow.

[Sclater et al.(2005)] Sclater J.G., Grindlay N.R., Madsen J.A. and Rommevaux-Jestin C., *Tectonic interpretation of the Andrew Bain transform fault: SouthWest Indian Ocean*, 2005, G^3, Vol.6, 9.

[Torge (1989)] Torge W., *Gravimetry*, 1989, Walter De Gruyter, Berlin-NY.

[Wessel and Smith (1995)] Wessel P. and Smith W.H.F., *New version of the Generic Mapping Tool released*, EOS Trans. AGU, p.329, 1995, see also URL: gmt.soest.hawaii.edu.

[Wilson (1965)] Wilson T.J., *Transform faults, Oceanic ridges, and magnetic anomalies of southwest Vancouver Island.*, 1965, Science 150: 482-485.

7 APPENDIX

7.1 GRAVIMETRIC DATA FILTERING

From [Panteleev (1983)], when just the vertical component of g has to be determined by a gravimeter, and the Eötvös and cross coupling effects may be neglected, the following method to estract the gravity signal from vertical accelerations can be used. Let the gravimeter be described by a linear system of the first-order and the input signal being the sum of gravity $g(t)$ and of platform vertical accelerations $u(t)$:

$$\tau\dot{x}(t) + x(t) = g(t) + u(t) \tag{1}$$

It is therefore possible to detect field gravity variations from the background system noise due to difference in their frequency spectra. We want to design a filter with impulse response w_0 and output

$$\tilde{g}(t) = \int_{-\infty}^{+\infty} w_0(\xi)\Big[g(t+\xi) + w(t+\xi)\Big]d\xi \tag{2}$$

and where the filter minimizes the error $e^2(t) = [g(t) - \tilde{g}(t)]^2$.

Taking into account that $w_0(\xi)$ tends to zero as ξ increases it is possible to transfer a signal from the output of a dynamic system to its input using 1 and 2:

$$\tilde{g}(t) = \int_{-\infty}^{+\infty} w_0(\xi)\big[x(t+\xi) + \tau\dot{x}(t+\xi)\big]d\xi = \int_{-\infty}^{+\infty} \big[w_0(\xi) - \tau\dot{w}_0(\xi)\big]x(t+\xi)d\xi \tag{3}$$

The impulse response of the filter is defined now by transformation

$$w(t) = w_0(t) - \tau\dot{w}_0(t) \tag{4}$$

using the Panteleev's normalized weight function

$$w_0(t) = \frac{\omega_0}{8}exp\bigg(-\omega_0\frac{|t|}{\sqrt{2}}\bigg)\bigg[\frac{3}{\sqrt{2}}\cos\frac{\omega_0 t}{\sqrt{2}} + \bigg(\omega_0|t| + \frac{3}{\sqrt{2}}\bigg)\sin\frac{\omega_0|t|}{\sqrt{2}}\bigg] \tag{5}$$

with frequency characteristic response

$$A(\omega) = \frac{\omega_0^8}{(\omega^4 + \omega_0^4)^2} \tag{6}$$

where ω is the angular frequency and

$$\omega_0 = 0.0045\frac{1}{sec} \tag{7}$$

hence the filter becomes

$$w(t) = \frac{\omega_0}{8}exp\bigg(\frac{-\omega_0|t|}{\sqrt{2}}\bigg)\bigg[\frac{1}{\sqrt{2}}(3 + \omega_0^2 t\tau)\cos\frac{\omega_0 t}{\sqrt{2}} + \frac{1}{\sqrt{2}}(3 - \omega_0^2 t\tau)\sin\frac{\omega_0|t|}{\sqrt{2}} + \omega_0(t - 2\tau)\sin\frac{\omega_0 t}{\sqrt{2}}\bigg] \tag{8}$$

This method was used to restore the gravity signal from the observed data.

7.2 SOFTWARE SCRIPTS AND PROGRAMS

7.3 ROCK SUBSAMPLING AND DESCRIPTION

S2317	S2317-01	30x20x20	basalt	Sector of pillow basalt with fresh glassy crust. Rare plagioclase phenocrysts. Slightly vesicular. Vesicles are empty/clean.	-	
S2317	S2317-02	27x20x13	basalt	Sector of pillow basalt with fresh glassy crust. Rare plagioclase phenocrysts. Plg up to 2-3 mm. Slightly vesicular. Vesicles are empty/clean. Thick rim of alteration	-	
S2317	S2317-03	30x15x15	basalt	sector of pillow basalt with fresh glassy crust. Rare plg phenocryst up to 0.5 cm. slightly vesicular. Vesicles are empty.	-	
S2317	S2317-04	15x20x12	basalt	same as S2317-03	-	
S2317	S2317-05	22x12x12	basalt	same as S2317-03	-	
S2317	S2317-06	16x15x10	basalt	sector of pillow basalt, aphyric with rare small plg, glassy crust, slightly vesicular. Thick rim of alteration	-	
S2317	S2317-07	20x15x15	basalt	same as S2317-06 but fresh	-	
S2317	S2317-08	15x10x10	basalt	rather fresh aphyric pillow sector with fresh glassy crust	-	
S2317	S2317-09	12x10x8	basalt	same as S2317-08	-	
S2317	S2317-10	11x7x9	basalt	pillow basalt with glassy crust	italy	no cu
S2317	S2317-11	16x7x7	basalt	aphyric pillow basalt with glassy crust, slightly vesicular	-	
S2317	S2317-12	12x10x8	basalt	same as S2317-11	-	
S2317	S2317-13	11x8x8	basalt	pillow basalt with glassy crust	russia	not cu
S2317	S2317-14	11x11x8	basalt	same as S2317-03	italy	not cu
S2317	S2317-15	12x11x6	basalt	same as S2317-03	russia	not cu
S2317	S2317-16	19x10x7	basalt	same as S2317-03	russia	not cu
S2317	S2317-17	11x5x4	basalt	same as S2317-03	italy	not cu
S2317	S2317-18	8x5x5	basalt	same as S2317-03	russia	not cu
S2317	S2317-19	10x9x7	basalt	same as S2317-03	italy	not cu
S2317	S2317-20	11x6x5	basalt	same as S2317-03	russia	not cu
S2317	S2317-21	18x5x5	basalt	same as S2317-03	italy	not cu
S2317	S2317-22	12x11x6	basalt	same as S2317-03	russia	not cu
S2317	S2317-23	12x11x9	basalt	same as S2317-03	italy	not cu
S2317	S2317-24	17x10x5	basalt	same as S2317-03	russia	not cu
S2317	S2317-25	11x7x7	basalt	same as S2317-03	italy	not cu
S2317	S2317-26	12x7x8	basalt	same as S2317-03	russia	not cu
S2317	S2317-27	11x11x7	basalt	same as S2317-03	russia	not cu
S2317	S2317-28	13x8x4	basalt	same as S2317-03	italy	not cu
S2317	S2317-29	15x8x7	basalt	same as S2317-03	russia	not cu
S2317	S2317-30	10x9x4	basalt	same as S2317-03	italy	not cu
S2317	S2317-31	8x6x4	basalt	same as S2317-03	italy	not cu
S2317	S2317-32	11x9x5	basalt	same as S2317-03	russia	not cu
S2317	S2317-33	6x5x4	basalt	same as S2317-03	italy	not cu
S2317	S2317-34	7x6x5	basalt	same as S2317-03	russia	not cu
S2317	S2317-35	8x8x5	basalt	same as S2317-03	italy	not cu
S2317	S2317-36	8x7x7	basalt	same as S2317-03	russia	not cu
S2317	S2317-37	9x8x4	basalt	same as S2317-03	russia	not cu
S2317	S2317-38	18x11x7	basalt	same as S2317-03	italy	not cu
S2317	S2317-39	11x8x6	basalt	same as S2317-03	italy	not cu

S2317	S2317-40	10x9x7	basalt	same as S2317-03	russia	not cut
S2317	S2317-41	12x6x6	basalt	same as S2317-03	russia	not cut
S2317	S2317-42	13x7x7	basalt	same as S2317-03	italy	not cut
S2317	S2317-43	9x7x5	basalt	same as S2317-03	italy	not cut
S2317	S2317-44	9x8x6	basalt	same as S2317-03	russia	not cut
S2317	S2317-50	9x6x5	basalt	same as S2317-03	russia	not cut
S2317	S2317-51	9x6x5	basalt	same as S2317-03	italy	not cut
S2317	S2317-52	7x6x5	basalt	same as S2317-03	italy	not cut
S2317	S2317-53	5x5x3	basalt	same as S2317-03	russia	not cut
S2317	S2317-54	5x5x4	basalt	same as S2317-03	russia	not cut
S2317	S2317-55	6x5x4	basalt	same as S2317-03	italy	not cut
S2317	S2317-56	2x2x3	basalt	glassy crust with plagioclase phenocrysts	italy	not cut
S2317	S2317-57	7x6x4	basalt	same as S2317-03	italy	not cut
S2317	S2317-58	5x5x3	basalt	same as S2317-03	russia	not cut
S2317	S2317-59	7x5x5	basalt	same as S2317-03	russia	not cut
S2317	S2317-60	7x4x2	basalt	same as S2317-03	italy	not cut
S2317	S2317-61	4x3x2	basalt	fresh glassy nodule	italy	not cut
S2317	S2317-62	4x4x2	basalt	fresh glassy nodule	italy	not cut
S2317	S2317-63	17x14x14	basalt	aphyric pillow basalt, slightly vesicular, no glass	-	-
S2317	S2317-64	10x9x9	basalt	same as S2317-63	-	-
S2317	S2317-65	9x8x8	basalt	aphyric pillow basalt with rare vesicles, variolitic structure	-	-
S2317	S2317-66	14x7x5	basalt	aphyric pillow basalt with strongly altered domains	-	-
S2317	S2317-67	8x6x5	basalt	same as S2317-63	-	-
S2317	S2317-68	8x7x6	basalt	aphyric pillow basalt, rare vesicles, rare plg phenocrysts up to 0.5 cm	-	-
S2317	S2317-69	8x6x4	basalt	same as S2317-68	italy	-
S2317	S2317-70	7x5x4	basalt	same as S2317-63	italy	-
S2317	S2317-71	6x5x4	basalt	same as S2317-68	italy	-
S2317	S2317-72	11x7x6	basalt	altered aphyric basalt	italy	-
S2317	S2317-73	14x7x6	basalt	same as S2317-68	italy	-
S2317	S2317-74	9x7x6	basalt	vesicular basalt similar to S2317-63	-	-
S2317	S2317-75	8x7x5	basalt	same as S2317-65	italy	-
S2317	S2317-76	8x5x5	basalt	same as S2317-65	italy	-
S2317	S2317-77	8x5x4	basalt	vesicular basalt with vesicles filled by secondary minerals	italy	-
S2317	S2317-78	8x6x4	basalt	same as S2317-74 but more altered	-	-
S2317	S2317-79	4x3x2	basalt	same as S2317-74	italy	-
S2317	S2317-80	9x4x3	basalt	plg poprhyric basalt. Plg up to 0.4 cm	italy	-
S2317	S2317-81	11x8x4	basalt	aphyric basalt with red rim of alteration	italy	-
S2317	S2317-82	6x4x4	basalt	plg porphyric basalt. Slightly vesicular with vesicles filled by secondary minerals. Plg phenocrysts up to 7 mm	-	-
S2317	S2317-83	3x3x2	basalt	aphyric altered basalt cut by secondary veins	-	-
S2317	S2317-84	6x3x3	dolerite	dolerite with rare plg, altered	-	-
S2317	S2317-85	8x6x5	basalt	glass nodule, fractured	-	-
S2317	S2317-86	11x7x7	basalt	aphyric basalt partially altered	-	-

S2317	S2317-87	2x2x2	basalt	slightly vesicular fresh basalt with fresh glassy crust	-
S2317	S2317-88	3x2x2	basalt	fresh aphyric basalt	-
S2317	S2317-90	4x3x2	basalt	aphyric basalt	-
S2317	S2317-91	4x3x2	basalt	aphyric basalt	-
S2317	S2317-92	6x5x1	basalt	rare plg porphyric basalt, slightly vesicular and altered	-
S2317	S2317-93	6x5x5	basalt	pillow basalt with huge plg xenocryst. Fresh glassy crust	-
S2317	S2317-94	4x3x3	basalt	altered basalt	-
S2317	S2317-95	4x3x2	basalt	altered porphyric basalt	-
S2317	S2317-96	6x3x2	basalt	same as S2317-95	-
S2317	S2317-97	4x3x2	basalt	same as S2317-95	-
S2317	S2317-98	5x3x2	basalt	same as S2317-95	-
S2317	S2317-99	5x3x2	basalt	same as S2317-95	-
S2317	S2317-100	2x1x1	basalt	same as S2317-95	-
S2317	S2317-101	10x5x4	basalt	same as S2317-95	-
S2317	S2317-103	7x4x4	basalt	same as S2317-95	-
S2317	S2317-104	8x4x4	basalt	same as S2317-95	-
S2317	S2317-105	16x11x3	basalt	altered brecciated porphyric basalt	-
S2317	S2317-106	5x3x1.5	basalt	brecciated altered basalt	-
S2317	S2317-107	5x4x4	basalt	altered basalt with sulphides filling the vesicles	-
S2317	S2317-108	5x5x1	basalt	altered aphyric basalt	-
S2317	S2317-109	4x2x1.5	basalt	altered basalt	-
S2317	S2317-110	4x2x1	basalt	altered basalt	-
S2317	S2317-111	3x2x1	basalt	altered basalt	-
S2317	S2317-112	3x2x1	basalt	altered basalt	-
S2317	S2317-113	5x3x2	breccia	altered basaltic breccia	-
S2317	S2317-114	4x3x2	basalt	altered basalt	-
S2317	S2317-115	8x5x5	breccia	altered basaltic breccia	-
S2317	S2317-116	6x4x2	basalt	strongly altered basalt	-
S2317	S2317-117	8x6x1	basalt	strongly altered basalt	-
S2317	S2317-118	3x2x2	breccia	altered basaltic breccia	-
S2317	S2317-119	12x10x3	basalt	strongly altered basalt	-
S2317	S2317-120	6x5x1.5	basalt	altered poprhyroclastic basalt	-
S2317	S2317-121	6x2x1	basalt	altered vesicular basalt	-
S2317	S2317-122	3x2x2	dolerite	altered dolerite	-
S2317	S2317-123	2x1x1	dolerite	same as S2317-122	-
S2317	S2317-124	6x4x1.5	basalt	altered vesicular basalt	-
S2317	S2317-126	8x5x5	gabbro	medium grained	-
S2317	S2317-127	5x3x2	gabbro	coarse grained, slightly brecciated	-
S2317	S2317-129	3x3x2	gabbro	very altered	-
S2317	S2317-130	4x1x1	gabbro	fine grained, altered	-
S2317	S2317-131	3x2x1	gabbro	fine grained	-
S2317	S2317-133	1.5x0.5x0.5	basalt	Plg poprhyric altered basalt	-
S2317	S2317-134	various small		various small pieces of altered basalt	-
S2317	S2317-135	6x4x3	peridotite	serpentinized peridotite. Relics of opx fresh up to 1 cm. relics of spinels. Black type serpentine.	-
S2317	S2317-136	5x4x2	breccia	basaltic breccia covered with Fe-Mn crust	Italy
S2317	S2317-137	5x3x2	breccia	basaltic breccia covered with Fe-Mn crust	Russia

S2317	S2317-138	7x4x3	breccia	basaltic breccia with small pieces of fresh glass in the matrix	-	-
S2317	S2317-139	6x4x1.5	crust	Fe-Mn crust	-	-
S2318	S2318-02	22x17x14	gabbro	fresh, coarse to medium grained gabbro, olivine	-	-
S2318	S2318-03	18x14x12	gabbro	pegmatitic to coarse grained gabbro, large px oikocrysts up to 3 cm. fresh	-	-
S2318	S2318-04	14x10x7	gabbro	coarse to medium grained, slightly altered	-	-
S2318	S2318-05	8x7x5	gabbro	same as S2318-04	-	-
S2318	S2318-06	7x4x4	gabbro	same as S2318-04	-	-
S2318	S2318-07	6x3x3	gabbro	same as S2318-04	-	-
S2318	S2318-08	12x6x6	gabbro	same as S2318-04	-	-
S2318	S2318-09	9x7x6	gabbro	same as S2318-04	-	-
S2318	S2318-10	10x6x5	gabbro	same as S2318-04	-	-
S2318	S2318-11	7x5x5	gabbro	same as S2318-04	-	-
S2318	S2318-12	8x5x6	gabbro	same as S2318-04	-	-
S2318	S2318-13	6x6x4	gabbro	fine grained	-	-
S2318	S2318-14	9x7x4	gabbro	same as S2318-12	-	-
S2318	S2318-15	11x7x4	gabbro	olivine bearing gabbro/gabbro contact. Grain size decreases with olivine content. Olivine is altered	-	-
S2318	S2318-17	6x5x4	dolerite	pebble with ice marks	-	-
S2318	S2318-19	8x6x6	gabbro	same as S2318-04	-	-
S2318	S2318-20	13x10x7	gabbro vein	leucogabbro vein in altered peridotite. There is a large altered reaction zone around the leucovein. Late oxide rich ore levels	-	-
S2318	S2318-21	8x5x4	anorthosite	altered, sulphides	-	-
S2318	S2318-22	6x6x5	gabbro	ol-bearing gabbro. One 7-cm pyroxene oikocryst ebclosing pl chadocrysts. Altered	-	-
S2318	S2318-23	7x6x4	breccia	breccia of altered gabbroic and basaltic fragments	-	-
S2318	S2318-24	6x5x4	gabbro	altered leucogabbro	-	-
S2318	S2318-27	6x6x3	peridotite-gabbro contact	fresh cpx in peridotite	-	-
S2318	S2318-28	16x15x11	harzburgite	harzburgite cut by a 1-cm thick gabbroic vein. Serpentinized up to 80%	-	-
S2318	S2318-29	7x4x4	lherzolite	px-rich lherzolite cut by 3mm thick gabbroic veinlet. Cpx forms aggregates policrystalline cutting opx foliation by 20 degrees. Impregnated peridotite	-	-
S2318	S2318-30	11x10x8	lherzolite	px-poor lherzolite. Cpx forms aggregates elongated to form chains cutting peridotite foliation. Strongly altered	-	-
S2318	S2318-31	11x9x5	lherzolite	px-poor lherzolite same as S2418-30	-	-
S2318	S2318-33	11x9x9	lherzolite	lherzolite, cpx forms aggregated after impregnation. Plg? Cpx + plg aggregates. But plg seems more scattered	-	-

S2318	S2318-34	10x7x6	harzburgite	small veins of altered stuff possibly replacing 1 mm thick gabbroic (plg bearing) vein	-
S2318	S2318-35	11x5x4	lherzolite	cpx is possibly present because of impregnation. Round opx	-
S2318	S2318-36	10x6x5	harzburgite	same as S2318-35	-
S2318	S2318-38	13x9x6	lherzolite	cpx aggregates cuttin rock foliation. Cpx+plg scattered aggregates	-
S2318	S2318-39	10x7x6	lherzolite	same as previous S2318-38. Cut by 1 mm thick gabbroic vein	-
S2318	S2318-40	10x8x5	lherzolite	same as S2318-38	-
S2318	S2318-41	11x6x5	lherzolite	same as S2318-38	-
S2318	S2318-42	10x4x3	peridotite-dunite contact	the dunite is cut by thin veins (?)	-
S2318	S2318-43	8x5x3	lherzolite	same as S2318-38	-
S2318	S2318-44	6x5x4	lherzolite	same as S2318-38; possibly no plagioclase	-
S2318	S2318-46	10x8x5	lherzolite	cpx aggregates	-
S2318	S2318-49	8x7x7	lherzolite	high cpx/opx ratio. Opx poor peridotite. Locally cpx/opx=1	-
S2318	S2318-50	8x7x5	harzburgitic mylonite	strong mineral lineation marked by policrystalline aggregates of opx (altered?). Small dark green garins associated with opx (possibly amph?). Opx aggregates look like recrystallized after deformation	-
S2318	S2318-51	9x7x4	harzburgitic mylonite	same as previous sample cut in the foliation plane	-
S2318	S2318-52	7x5x3	harzburgite	harzburgite impregnated by abundant Pl patches	-
S2318	S2318-54	6x5x4	harzburgite	abundant plg patches; possibly cpx elongated aggregates	-
S2318	S2318-55	10x6x5	dunite	large spn patches possibly surrounded by Pl (or Chl). A set of thin iddingsite veins cut the Ol foliation	-
S2318	S2318-56	6x6x4	lherzolite	cpx-rich lherzolite with or without plagioclase. Large policrystalline cpx aggregates cut opx foliation. Small scattered Pl grains, associated with cpx. High px/ol ratio	-
S2318	S2318-57	6x5x4	lherzolite	same as S2318-56	-
S2318	S2318-58	9x6x5	lherzolite	same as S2318-56, plus Pl rich vein parallel to cpx foliation	-
S2318	S2318-59	6x5x4	lherzolite	same as S2318-56	-
S2318	S2318-60	6x4x3	lherzolite	same as S2318-56	-
S2318	S2318-61	6x5x4	lherzolite	same as S2318-56	-
S2318	S2318-62	17x15x13	breccia	dunitic breccia. Breccia is cemented by carbonatic ooze. Clasts of variably altered dunite. Large sp patches. The largest clast is probably fresh.	-
S2319	S2319-01	12x8x7	gabbro	leucogabbro or plagiogranite. Possibly erratic.	-
S2319	S2319-02	11x7x7	breccia	erratic breccia chert	-

S2323	S2323-01	28x18x4	mylonite	mylonitic peridotite	-	-
S2323	S2323-02	18x15x10	granitoid	quartz-garnet erratic	-	-
S2323	S2323-03	14x15x14	granitoid	quartz-kfeldspar (?) erratic	-	-
S2324	S2324-01	13x8x8	lherzolite	lherzolite, large cpx-spn. Spinel up to 3 mm. dark green cpx. Protogranular texture	-	-
S2324	S2324-02	9x5x4	lherzolite	lherzolite same as 24-01	-	-
S2324	S2324-03	13x6x6	harzburgite	harzburgite, no residual cpx	-	-
S2324	S2324-04	13x6x5	lherzolite	lherzolite. Large spinels	-	-
S2324	S2324-05	13x8x8	harzburgite	harzburgite cut by gabbroic veins	-	-
S2325	S2325-01	25x2421	lherzolite	lherzolite with high T foliation, marked by opx and cpx lineation. Cpx forms chains possibly by melt percolation ±sp. Maybe possible olivine. Opx 20%, cpx 5-10%. Opx 4-12 mm	-	-
S2325	S2325-02	25x19x11	harzburgite	strongly foliated harzburgite. Deeply altered, fractured. Fractures are filled with serpentine and calcite/aragonite	-	-
S2325	S2325-03	21x15x13	lherzolite	lherzolite with low opx content. Opx 10-15%; cpx is present as discrete grains. No evident lineation. Weak foliation. Large spinel up to 3 mm	-	-
S2325	S2325-04	12x11x8	lherzolite	weakly foliated lherzolite. Gabbroic vein in contact (be careful)	-	-
S2325	S2325-05	18x14x10	lherzolite	lherzolite with protomilonitic texture. Cpx rich bands in the center of the sample. Cpx forms elongated policrystalline patches associated with large rare spinel grains up to 2 mm	-	-
S2325	S2325-06	15x10x4	lherzolite	weakly foliated lherzolite, pyroxene poor, opx 10-15%. Opx and cpx grains are rounded	-	-
S2325	S2325-07	11x10x4	lherzolite	lherzolite similar to S2325-05, large elongated opx	-	-
S2325	S2325-08	10x9x4	lherzolite	lherzolite similar to S2325-05. look at the sp-pl (?) intergrowth marked on the sample	-	-
S2325	S2325-09	16x7x4	lherzolite	lherzolite similar to S2325-05	-	-
S2325	S2325-10	21x10x8	lherzolite	lherzolite similar to S2325-05; rounded small opx and cpx, strongly foliated	-	-
S2325	S2325-11	14x10x4	lherzolite	lherzolite, opx poor, very large spinel marked on the surface. Fresh olivine (?)	-	-
S2325	S2325-12	30x9x8	lherzolite	lherzolite, pyroxene poor, large spinels	-	-
S2325	S2325-13	10x10x4	lherzolite	lherzolite similar to S2325-06	-	-
S2325	S2325-14	6x4x4	lherzolite	lherzolite with large spinel (0.5 cm). Elongated cpx and rounded opx	-	-
S2325	S2325-15	6x4x4	lherzolite	lherzolite, rounded cpx and opx	-	-

S2325	S2325-16	8x7x3	lherzolite	lherzolite, granular to weakly foliated texture, px rich, spinel trains	-
S2325	S2325-17	13x8x4	lherzolite	lherzolite, px poor, 2-3 mm spinels, fresh olivine, weak foliation	-
S2325	S2325-18	13x7x5	lherzolite	foliated lherzolite, px poor, cpx is dark green	-
S2325	S2325-19	17x11x9	lherzolite	lherzolite, px rich, opx up to 1 cm, cpx are generally smaller (0.5 cm), granular texture	-
S2325	S2325-20	12x10x6	lherzolite	lherzolite similar to S2325-05, cpx forms elongated policrystalline patches. Small sp	-
S2325	S2325-21	12x6x6	lherzolite	lherzolite, px rich, granular to foliated texture. Cpx is dark green	-
S2325	S2325-22	15x10x7	lherzolite	lherzolite similar to S2325-21, px rich, gabbroic (?) impregnation	-
S2325	S2325-23	14x12x6	lherzolite	lherzolite similar to S2325-21	-
S2325	S2325-24	14x10x7	lherzolite	lherzolite similar to S2325-04	-
S2325	S2325-25	16x10x8	lherzolite	lherzolite similar to S2325-04, weak foliation	-
S2325	S2325-26	24x12x9	harzburgite	harzburgite with layers rich in cpx. Cpx is small or elongated in policrystalline aggregates. 30-40% opx. Weak foliation. Aragonite veins cut the upper portion of the sample which can be considered an oficalcite.	-
S2325	S2325-27	13x8x3	lherzolite	lherzolite similar to S2325-05	-
S2325	S2325-28	11x7x4	lherzolite	lherzolite, px poor	-
S2325	S2325-29	18x11x8	lherzolite	lherzolite similar to S2325-10 but with less px. Aragonite veins replacing milonitic domain?	-
S2325	S2325-30	26x22x8	lherzolite	lherzolite similar to S2325-10. more altered	-
S2325	S2325-31	17x10x8	lherzolite	altered peridotite, foliated similar to S2325-30	-
S2325	S2325-32	11x7x7	lherzolite	peridotite similar to S2325-31	-
S2325	S2325-33	30x17x13	lherzolite	altered foliated peridotite similar to S2325-32 but more foliated and strongly weathered	-
S2325	S2325-34	19x10x8	lherzolite	lherzolite similar to S2325-01, with less cpx and more weathered	-
S2325	S2325-35	16x10x5	lherzolite	lherzolite similar to S2325-05	-
S2325	S2325-36	13x10x6	lherzolite	lherzolite similar to S2325-02, less weathered; fresh cpx	-
S2325	S2325-37	19x18x9	lherzolite	lherzolite similar to S2325-01, less cpx. Domains enriched in opx up to 1 cm associated with 0.5 cm spn. 2 cm thick gabbroic vein.	-
S2325	S2325-38	7x6x5	lherzolite	lherzolite strongly foliated, dark green cpx	-
S2325	S2325-39	17x14x8	lherzolite	lherzolite similar to S2325-01	-
S2325	S2325-40	15x10x10	lherzolite	lherzolite similar to S2325-03, big spn	-

S2325	S2325-41	10x6x5	lherzolite	lherzolite similar to S2325-03 (looks like a piece of # S2325-03)	-	-
S2325	S2325-42	14x6x4	lherzolite	lherzolite similar to S2325-03, big spn	-	-
S2325	S2325-43	13x6x5	lherzolite	lherzolite weakly foliated, fine grain size of cpx and opx	-	-
S2325	S2325-44	10x7x6	lherzolite	lherzolite same as S2325-18, foliated, less cpx	-	-
S2325	S2325-45	11x10x4	harzburgite	harzburgite similar to S2325-44, foliated	-	-
S2325	S2325-46	9x8x8	lherzolite	altered foliated peridotite similar to S2325-33	-	-
S2325	S2325-47	21x10x10	lherzolite	altered foliated peridotite similar to S2325-46	-	-
S2325	S2325-48	13x10x2	lherzolite	lherzolite similar to S2325-10. plg patches.	-	-
S2325	S2325-49	13x5x4	harzburgite	harzburgite with plagioclase patches	-	-
S2325	S2325-50	7x6x5	lherzolite	lherzolite with milonitic texture	italy	-
S2325	S2325-51	10x6x5	lherzolite	lherzolite, dark green cpx similar to S2325-21	italy	-
S2325	S2325-53	12x7x4	dunite	strongly weathered	-	-
S2325	S2325-54	11x6x6	pyroxenite	Ol-pyroxenite, fresh dark green cpx, small spn	-	-
S2325	S2325-55	8x6x3	pyroxenite	same as S2325-54	-	-
S2325	S2325-56	8x5x4	gabbro	gabbro hydrothermally altered, noce green amph (Chl?)	-	-
S2325	S2325-57	8x3x2	pyroxenite	same as S2325-54	-	-
S2325	S2325-58	8x5x4	siltstone?	siltstone with 2 mm thick cemented mud	-	-
S2325	S2325-59	17x7x7	oficalcite	brecciated peridotite cemented by calcite/aragonite	-	-
S2325	S2325-60	9x7x5	oficalcite	same as S2325-60	-	-
S2325	S2325-61	9x3x2	oficalcite	same as S2325-60	-	-
S2325	S2325-62	6x4x1	oficalcite	same as S2325-60	-	-
S2325	S2325-63	8x3x2	oficalcite	same as S2325-60	-	-
S2325	S2325-64	7x4x3	oficalcite	same as S2325-60	-	-
S2325	S2325-65	8x5x3	oficalcite	same as S2325-60	-	-
S2325	S2325-66	5x4x2	peridotite	strongly altered serpentinite	-	-
S2325	S2325-67	8x4x3	pyroxenite	strongly altered ortopyroxenite	-	-
S2325	S2325-68	7x3x3	peridotite	strongly altered peridotite with hydrogarnet (? pink mineral)	-	-
S2325	S2325-69	10x7x5	granite	erratic granit (Qtz+Plg)	-	-
S2325	S2325-70	8x6x4	granite	biotite rich erratic granite	-	-
S2326	S2326-01	40x30x30	lherzolite	lherzolite cut by pyroxenite vein. Altered Pl patches dispersed in the matrix. Cpx is shut. Opx relics. Pl is more abundant closer to the vein. Granular texture	-	-
S2326	S2326-02	15x9x4	lherzolite	lherzolite similar to S2326-01, with more abundant Pl (3 %) scattered in the matrix	-	-
S2326	S2326-03	9x6x4	lherzolite	lherzolite similar to S2326-01, Pl is associated with spinel	-	-
S2326	S2326-04	7x6x6	lherzolite	lherzolite similar to S2326-03	-	-
S2326	S2326-05	6x5x4	lherzolite	lherzolite similar to S2326-03	-	-
S2326	S2326-06	7x6x3	lherzolite	lherzolite similar to S2326-03, Px are bigger, up to 1 cm	-	-

S2326	S2326-07	9x6x5	lherzolite	lherzolite similar to S2326-03, cpx is fresh	-
S2326	S2326-08	11x7x6	lherzolite	lherzolite similar to S2326-07, Pl scattered in the matrix	-
S2326	S2326-09	9x7x6	lherzolite	lherzolite similar to S2326-08, less Pl	-
S2326	S2326-10	6x5x4	lherzolite	lherzolite similar to S2326-08, abundant Px	-
S2326	S2326-11	9x8x5	lherzolite	lherzolite similar to S2326-10, Pl is associated with spn, some is scattered in the matrix	-
S2326	S2326-12	14x11x8	lherzolite	lherzolite similar to S2326-02, Pl is associated with spn, some scattered	-
S2326	S2326-13	11x8x6	lherzolite	strongly altered lherzolite similar to S2326-01, Pl is scattered	-
S2326	S2326-14	12x10x6	lherzolite	lherzolite similar to S2326-01, more weathered. Pl is associated with Px	-
S2326	S2326-15	11x10x9	lherzolite	lherzolite similar to S2326-01 but very fresh and no Pl	-
S2326	S2326-16	9x7x5	lherzolite	lherzolite with fresh cpx similar to S2326-15	-
S2326	S2326-17	8x6x5	lherzolite	lherzolite similar to S2326-16	-
S2326	S2326-18	11x8x4	lherzolite	lherzolite similar to S2326-16, more weathered, cpx shut	-
S2326	S2326-19	10x5x4	lherzolite	lherzolite. Most cpx and opx are rounded. Some elongated cpx form elogated chains	-
S2326	S2326-20	10x4x3	lherzolite	lherzolite; fresh px but serpentine is strongly weathered	-
S2326	S2326-21	8x5x4	lherzolite	lherzolite; pyroxenes look readsorbed; intergranular texture?; cpx is dark green	-
S2326	S2326-22	8x5x4	peridotite	serpentinized peridotite, weathered, fresh opx. Ol?	-
S2326	S2326-23	10x6x3	lherzolite	weathered lherzolite. Some cpx and opx are fresh. Lots of serpentine veins	-
S2326	S2326-24	8x6x4	lherzolite	lherzolite similar to S2326-21, dark serpentine and very abundant green cpx. Intergranular texture?	-
S2326	S2326-25	9x9x4	lherzolite	lherzolite similar to S2326-24, more altered. Cpx shut	-
S2326	S2326-26	13x10x6	lherzolite	lherzolite with gabbroic intrusion or some sort of high T melt intrusion. Cpx is still fresh. Intrusion seems altered.	-
S2326	S2326-27	10x6x6	lherzolite	serpentinized peridotite with gabbroic intrusion similar to S2326-26. more weathered. Rare pl associated with pyroxene.	-
S2326	S2326-28	9x6x4	lherzolite	fresh lherzolite cut by lots of serpentine veins	-

S2326	S2326-29	12x10x6	lherzolite	fresh lherzolite surrounded by serpentine veins (?) similar to S2326-28. maybe after a system of cracks in fresh peridotite filled with tardive serpentine	-	-
S2326	S2326-30	10x8x5	peridotite	weathered peridotite cut by serpentine veins	-	-
S2326	S2326-31	11x6x5	lherzolite	lherzolite with stretched opx and cpx; milonite (?)	-	-
S2326	S2326-32	8x7x5	peridotite	peridotite similar to S2326-30	-	-
S2326	S2326-33	6x5x5	basalt	vesicular aphyric basalt; vesicles are bundant and have irregular shape,	-	-
S2326	S2326-34	4x4x3	basalt	vesicular aphyric basalt; very fine vesicles	-	-
S2326	S2326-35	6x5x4	basalt	aphyric basalt; very fine vesicles; rare small plg	-	-
S2326	S2326-36	18x14x8	basalt	altered basalt	-	-
S2326	S2326-37	9x7x5	basalt	altered basalt	-	-
S2326	S2326-39	30x20x15	basalt	Pl-porphyric basalt; Pl crystals up to 4mm. Slightly vesicular. Vesicles are empty and have irregular shape	-	-
S2327	S2327-01	8x7x6	basalt	basalt pebble. Rounded shape. Aphyric with rare vesicles. Thick alteration rim	-	-
S2327	S2327-02	28x15x15	erratic granitoid	erratic granitoid	-	-
S2329	S2329-01	14x11x8	gabbro	rounded sample of Ol gabbro partially covered by thin FeMn film. Probably erratic material	-	-